AUS DEM INSTITUT FÜR EXPERIMENTELLE PNEUMOLOGIE

LUDWIG-MAXIMILIANS-UNIVERSITÄT MÜNCHEN

LEITUNG: PROF. DR. OLIVER EICKELBERG

PROLYL-3-HYDROXYLASE 1 IN IDIOPATHIC PULMONARY FIBROSIS

DISSERTATION

ZUM ERWERB DES DOKTORGRADES DER MEDIZIN

AN DER MEDIZINISCHEN FAKULTÄT DER

LUDWIG-MAXIMILIANS-UNIVERSITÄT ZU MÜNCHEN

VORGELEGT VON

LEONHARD BINZENHÖFER

AUS WÜRZBURG

2021

Mit Genehmigung der Medizinischen Fakultät

der Universität München

Berichterstatter:	Prof. Dr. Oliver Eickelberg
Mitberichterstatter:	Prof. Dr. Jürgen Behr
Mitberichterstatter:	Prof. Dr. Rudolf Hatz
Mitberichterstatter:	Prof. Dr. Alexander Dietrich
Mitbetreuung durch die promovierte Mitarbeiterin:	PD Dr. Claudia Staab-Weijnitz
Dekan:	Prof. Dr. Reinhard Hickel
Tag der mündlichen Prüfung:	11.03.2021

TABLE OF CONTENTS

1 Abstract 4

1.1 English version 4

1.2 Deutsche Version 5

2 Introduction 6

2.1 Epidemiology, management and prognosis of IPF 6

2.2 Current knowledge on the mechanism of antifibrotic drugs and collagen deposition 6

2.3 Pathophysiological relevance of prolyl-3-Hydroxylases P3H1, P3H2 and the coenzyme CRTAP 7

3 Materials and Methods 9

3.1 Materials 9

3.1.1 Laboratory equipment and Software 9

3.1.2 Chemicals, Reagents and Kits 10

3.1.3 Cells 12

3.1.4 Media 13

3.1.5 Consumables 13

3.1.6 Primer 14

3.1.7 siRNA and microRNA 15

3.1.8 Antibodies 15

3.1.9 Buffers and recipes 17

3.2 Methods 18

3.2.1 Biobank and ethical guidelines for human sample retrieval 18

3.2.2 Cell culture 19

3.2.2.1 Primary human lung fibroblasts 19

3.2.2.2 Primary human bronchial epithelial cells 19

3.2.2.3 pHBEC differentiation at the Air-Liquid-Interface 20

3.2.2.4 siRNA-transfection 21

3.2.2.5 Treatment with microRNA29b-inhibitor and -precursor 21

3.2.2.6 Treatment with TGFß-1 21

3.2.2.7 Treatment with tunicamycin and thapsigargin 22

3.2.2.8 BrdU cell proliferation assay 22

3.2.3 RNA analysis 22

3.2.3.1 RNA-extraction and cDNA-transcription 22

3.2.3.2 Primerdesign 23

3.2.3.3 Quantitative real-time-PCR 23

3.2.3.4 mRNA analysis in miR-stimulated cells 24

3.2.3.5 MicroRNA analysis in miR-stimulated cells 25

3.2.4 Protein analysis 26

3.2.4.1 Protein extraction and concentration determination 26

3.2.4.2 SDS-PAGE, western blot and immunochemical protein detection 26

3.2.4.3 Western Blot analysis in miR29b treated cell lysates 27

3.2.4.4 Collagen detection in cell culture supernatants 28

3.2.5 Imaging of lung tissue and cultured cells 28
3.2.5.1 Immunofluorescence staining of human lung tissue 28
3.2.5.2 Immunoflourescence staining of pHBECs cultured on transwell membranes 29

4 Results 30

4.1 Reverse knockdown of P3H1, P3H2 and CRTAP in phLF confirms antibody and siRNA-specificity 30

4.2 P3H1 as well as a P3H2-variant are upregulated in IPF total lung homogenates 31

4.3 P3H1 is present in p63-positive basal cells in IPF 31
4.3.1 Co-stainings with lung cell markers display P3H1 to be present in p63- and Krt14-positive basal cells in IPF tissue 31
4.3.2 P3H1 expression decreases during pHBEC differentiation into specialized bronchial epithelium *in vitro* 33

4.4 P3H1 is regulated by ER-stress inducers, TGFß-1, and miR29b 35
4.4.1 ER-stress-inducing agents tunicamycin and thapsigargin partially downregulate P3H1 in submerged pHBECs 35
4.4.2 TGFß-1 increases P3H1 protein and transcript expression in pHBECs after 24 hours 37
4.4.3 pHBEC treatment with a miRNA29b inhibitor and precursor showed P3H1-regulation 38

4.5 Evaluation of miR29b and collagen secretion in TGFß-1-stimulated pHBECs 38

4.6 P3H1 silencing experiments in pHBECs 40
4.6.1 Reverse knockdown in differentiating bronchial epithelial cells shows silencing of P3H1 on protein and transcript level for 192 hours 40
4.6.2 Reverse transfection with P3H1 siRNA in submerged pHBECs succeeded in P3H1-silencing for 72 hours 42

4.7 Functional Assays display the influence of P3H1 on basal cell marker expression and pHBEC proliferation in vitro 43
4.7.1 p63 is upregulated upon P3H1-knockdown in pHBECs 43
4.7.2 P3H1 knockdown decreases proliferation of submerged pHBECs in presence of TGFβ-1, but does not affect PCNA levels 43

5 Discussion 46

5.1 Expression and distribution of P3H1 in IPF 46

5.2 Regulation of P3H1 in pHBECs 48

5.3 Functional analysis of P3H1 in bronchial epithelial cells 49

6 Conclusion 52

7 Acknowledgements 53

8 Appendix 54

8.1 Abbreviations 54

8.2 List of figures 57

8.3 List of tables 58

8.4 Publications and presentations 59
8.4.1 Publications 59

8.4.2 Oral Presentations 59

9 Eidesstattliche Erklärung 60

10 References 61

1 ABSTRACT

1.1 *ENGLISH VERSION*

Idiopathic pulmonary fibrosis (IPF) is a devastating lung disease with survival rates worse than most types of cancer. The disease is characterized histologically by excessive extracellular matrix deposition, predominantly consisting of collagen. Collagen enzymes are of particular interest in search of novel drug targets, because crosstalk of modified extracellular matrix and myofibroblasts further drives fibrotic change. A previously published proteomics dataset found a group of collagen prolyl hydroxylases, prolyl-3-hydroxylase 1 (P3H1), prolyl-3-hydroxylase 2 (P3H2) and cartilage-associated protein (CRTAP), which were highly expressed in bleomycin induced lung fibrosis in mice. In human IPF and healthy control samples from two international cohorts, only P3H1 was elevated on protein level in total lung lysates. Co-expression stainings of fibrotic lungs with markers of epithelial and interstitial cells located P3H1 in $p63^+$ / $Krt14^+$ basal cells of the bronchial epithelium, indicating the presence of bronchial epithelial progenitor cells with an altered expression profile in IPF. In addition, airways featuring the $P3H1^+$ / $p63^+$ / $Krt14^+$ progenitor cell subset displayed a distinct morphology and remarkably also showed complete absence of specialized epithelial cells. *In vitro* regulation assays on primary human bronchial epithelial cells (pHBECs) isolated from healthy individuals showed upregulation of P3H1 on protein level by TGFß-1 and microRNA29b, both of which are known pro-fibrotic factors mediating matrix deposition in IPF. P3H1 depletion in pHBECs resulted in decreased proliferation rates and upregulation of p63, a key transcription factor for differentiation and regeneration of the bronchial epithelium. Whether P3H1 expression in basal cells is directly involved in the formation of a defective airway epithelium in IPF and if this process is linked to the development of honeycomb cysts, remains to be determined.

1.2 *DEUTSCHE VERSION*

Die idiopathische Lungenfibrose (Idiopathic pulmonary fibrosis, IPF) ist eine schwerwiegende Lungenerkrankung, deren Überlebensrate niedriger ist, als die der meisten Tumorerkrankungen. Histologisch zeigt sich eine überschießende Ablagerung von Extrazellulärmatrix, die zum großen Teil aus Kollagen besteht. Für die Erforschung neuer Behandlungsansätze sind Enzyme, welche an der Produktion und Modifikation von Kollagenen beteiligt sind, von großem Interesse, da die Interaktion veränderter Matrix mit Myofibroblasten den fibrotischen Umbau weiter antreibt. In einer vorausgegangenen Studie zum Proteom bei bleomycin-induzierter Lungenfibrose im Mausmodell konnte gezeigt werden, dass eine Gruppe von Kollagen-Prolyl-Hydroxylasen, Prolyl-3-Hydroxylase 1 (P3H1), Prolyl-3-Hydroxylase 2 (P3H2), sowie das Cartilage-associated Protein (CRTAP), hoch exprimiert ist. In humanen Proben von IPF-Patienten verglichen mit entsprechenden Kontrollen aus zwei internationalen Kohorten war nur P3H1 auf Proteinebene in Lungenlysaten erhöht. Immunfluoreszenz-Färbungen von fibrotischem Lungengewebe lokalisierte P3H1 in $p63^{+}$ / $Krt14^{+}$ Basalzellen, was auf einen speziellen Typ Progenitorzelle des Bronchialepithels mit einem veränderten Expressionsmuster in IPF schließen lässt. In kleinen Atemwegen, welche den $P3H1^{+}$ / $p63^{+}$ / $Krt14^{+}$ Zell-Subtyp aufweisen, konnte außerdem eine auffallende Morphologie beobachtet werden, sowie ein gänzliches Fehlen spezialisierter Bronchialepithelzellen. Zellkulturexperimente an primären humanen Bronchialepithelzellen (pHBECs) von gesunden Individuen zeigten eine Hochregulation von P3H1 auf Proteinebene durch die wichtigen pro-fibrotischen Faktoren TGFß-1 und microRNA29b, die beide an der Steuerung der Matrix-Ablagerung beteiligt sind. Die Suppression von P3H1 in pHBECs hatte eine verminderte Proliferationsrate der Zellen zur Folge, während p63, ein wichtiger Transkriptionsfaktor für die Ausdifferenzierung und Regeneration des Bronchialepithels, hochreguliert wurde. Ob die P3H1-Expression in Basalzellen direkt an der Bildung eines defekten Atemwegs-Epithels in IPF beteiligt ist, und ob dieser Prozess möglicherweise mit der Entwicklung der sogenannten Honigwabenlunge und der damit einhergehenden Zystenbildung zusammenhängt, bleibt Gegenstand zukünftiger Experimente.

2 INTRODUCTION

2.1 EPIDEMIOLOGY, MANAGEMENT AND PROGNOSIS OF IPF

Idiopathic pulmonary fibrosis (IPF) is the most common subtype of interstitial lung diseases (ILD), but still classifies as a rare disease entity with incidence rates of 0.22-8.8 cases per 100,000 in North America and Europe.[1–5] IPF predominantly affects older individuals, who may present with progressing dyspnea and exertional cough, objectified by spirometry findings of a restrictive lung condition and decreased diffusion capacity of carbon monoxide (DLCO).[6,7] Besides clinical features, standard diagnostic criteria include a usual interstitial pneumonia (UIP) pattern on high-resolution computed tomography (HRCT) and lung biopsies.[6] Before two novel antifibrotic agents pirfenidone and nintedanib were approved for IPF treatment in 2011 and 2014, median survival had ranged between 2-3 years after diagnosis.[8,9] Long-term data on outcomes is still pending, yet current publications estimate an extension of mean survival from 3.7 years in the placebo group to 11.6 years in nintedanib-treated patients and a survival benefit of 30% in pirfenidone-treated patients compared to controls.[10,11] These advances in tackling IPF are remarkable, but to date IPF remains incurable and disease burden still weighs heavy upon patients and health care systems.

2.2 CURRENT KNOWLEDGE ON THE MECHANISM OF ANTIFIBROTIC DRUGS AND COLLAGEN DEPOSITION

Both nintedanib and pirfenidone have been approved based on clinical phase 3 trials suggesting a deceleration of disease progression, specifically of forced vital capacity (FVC) decline.[12,13] The exact mechanism of their antifibrotic capacities, however, is still not fully understood.[14,15] Pirfenidone attenuated fibrotic changes in different animal models of organ fibrosis mainly through a decrease in production and activity of transforming growth factor β (TGFβ),[16] whereas nintedanib inhibits the receptor tyrosine kinases of platelet derived growth factor receptor (PDGF-R), fibroblast growth factor receptor (FGF-R) and vascular endothelial growth factor receptor (VEGF-R).[17]

In the lung and most other organs, collagen is an integral part of the extracellular matrix (ECM).[18] Collagen chains consist of repetitive amino-acid sequences, most commonly proline – aa – glycine and aa – hydroxyproline – glycine, with aa representing any amino-acid other than (hydroxy-)proline

and glycine.[19] Post-translational modifications inside the rough endoplasmic reticulum of premature protocollagen strands include lysyl- and prolyl-hydroxylation as well as glycosylation and protein disulfide isomerization.[20,21] Protocollagen chains are then secreted and form trimeric structures called tropocollagens, which ultimately assemble in collagen fibers, providing mechanical and thermal stability and scaffolding for lung endo- and epithelial cells.[18] The extracellular matrix, however, must also facilitate sufficient gas transfer through the alveolar septi, which only measure 2 µm in healthy lungs.[22] This delicate balance is jeopardized in lung conditions with excess collagen production, like IPF.[23]

Besides pro-apoptotic effects on epithelial cells, TGFβ regulates ECM-deposition by inducing myofibroblast differentiation and matrix degradation, but also directly stimulates collagen production through SMAD signaling pathways.[24,25] The role of VEGF in IPF is more controversial. Some studies proposed protective capacities towards epithelial cells, but inhibition of VEGF by nintedanib reduced collagen deposition as well as expression of pro-fibrotic genes, such as fibronectin, pro-collagen 1 and TGFβ-1.[26–28] The FGF signaling pathway has been demonstrated to decrease collagen production in fibroblasts derived from IPF lungs,[29] whereas PDGF conversely contributes to fibrogenesis by fibrocyte recruitment.[30,31] Many of these cytokines and pathways driving fibrosis are also involved in the fine tuning of matrix homeostasis in healthy lungs, which makes a fuller understanding of these regulatory systems critical to the pursuit of precision treatments for fibrotic lung disease.[32]

2.3 Pathophysiological relevance of prolyl-3-Hydroxylases P3H1, P3H2 and the coenzyme CRTAP

Prolyl-3-Hydroxylase 1 (P3H1), prolyl-3-hydroxylase 2 (P3H2) and cartilage associated protein (CRTAP) are involved in the maturation process of nascent protocollagen strands, more specifically hydroxylation of L-proline residues.[33–35] Whereas P3H1 targets basement membrane collagens type IV and V, P3H2 mainly modifies collagen type IV, but also type I.[33,35] CRTAP is not a direct collagen enzyme but stabilizes the hydroxylation complex together with P3H1 and facilitates hydroxylation.[34,36] P3H1 and CRTAP knockout mice show severe osteochondrodysplasia and recessive mutations in both genes are associated with osteogenesis imperfecta (OI), a disease characterized by collagen instability and bone brittleness.[37–40] In IPF lungs, altered post-translational modifications of collagens increase ECM stiffness and contribute to a profibrotic feedback loop involving TGFß and

other signaling pathways.[41,42] A proteomics study investigating the murine model of lung fibrosis discovered an increase of P3H1, P3H2 and CRTAP in fibrotic lung tissue.[43] This study aims to understand better the expression of these proteins in human IPF and their pathophysiological role in fibrotic lung disease.

3 MATERIALS AND METHODS

3.1 MATERIALS

3.1.1 LABORATORY EQUIPMENT AND SOFTWARE

TABLE 1: LABORATORY EQUIPMENT

Product	Manufacturer
-20 °C MediLine Freezer	Liebherr
-86 °C ULT Laboratory Freezer	Eppendorf
4 °C MediLine Fridge	Liebherr
Aqualine AL 12	Lauda
Axio Imager 2	Zeiss
Axiovert 40C	Zeiss
BBD 6220 CO_2-Incubator	Thermo Scientific
C1000 Thermal Cycler	BioRAD
CELLSTAR® Serological Pipettes	Greiner Bio-One
ChemiDoc™ MP System	BioRAD
Decloaking Chamber™	Biocare Medical
Eppendorf Research plus	Eppendorf
Eppendorf® Thermomixer Compact	Merck
Falcon® Pipet Controller	Corning
Herasafe™ KS	Thermo Fisher Scientific
Light Cycler	Roche
Liquid Nitrogen Cell Tank BioSafe 420SC	Cryotherm
LSE™ Mini Microcentrifuge	Corning
LSE™ Vortex Mixer	Corning
MIKRO 200R centrifuge	Hettich
Milli-Q® Advantage A10	Merck
Mini Trans-Blot® Electrophoretic Transfer Cell	BioRAD
Mini-PROTEAN® Tetra Cell	BioRAD
Mr. Frosty™ Freezing Container 5100-0001	Thermo Fisher Scientific
Multipette® E3x	Eppendorf
NanoDrop 1000 Spectrophotometer	Thermo Fisher Scientific

Newbauer Chamber, BLAUBRAND®	Brand
Polymax 1040 Shaker	Heidolph
PowerPac™ Basic Power Supply	BioRAD
QIAcube	Qiagen
Roll mixer	VWR International
ROTINA 420 R	Hettich
Stain Tray	Sigma-Aldrich
Sunrise™ Reader	Tecan
Trans-Blot® Turbo™ Transfer System	BioRAD
WTW™ inoLab™ 7110 pH Meter	Fisher Scientific

TABLE 2: SOFTWARE

Product	Manufacturer
Axio vision	Zeiss
Citavi 6	Citavi
Image Lab™ 3.0	BioRAD
Light cycler	Roche
Magellan V 7.2	Tecan
Microsoft Office 2019	Microsoft
Prism 5	GraphPad Software

3.1.2 CHEMICALS, REAGENTS AND KITS

TABLE 3: CHEMICALS AND REAGENTS

Product	Manufacturer	Cat#
4',6-Diamidino-2-phenyindole (DAPI)	Sigma-Aldrich	D9564-10MG
Ammonium Persulfate	Applichem	A1142
Ascorbate 0.1 mM	Sigma-Aldrich	49752-10G
Bovine Serum Albumin (BSA)	Sigma-Aldrich	A9418
Bromphenolblue	Applichem	A3640
Chemiluminescent substrates	Thermo Fisher Scientific	
- FEMTO		34096

- PICO		34087
- DURA		34076
- ECL		32209
Chloroform	Lab Alley	C2871
DMSO	Sigma-Aldrich	D4540
DNase I digestion buffer	Peqlab	12-1091-01
DTT Molecular biology grade	Applichem	A2948
Dulbecco's Phosphate-Buffered Saline (DPBS)	Thermo Fisher Scientific	14190144
Ethanol, EMSURE®	Merck	100983
Fetal bovine serum (FBS)	Pan Biotech	P-303702
Fluorescent mounting medium	Dako	S3023
GeneAmp™ 10X PCR Buffer II & $MgCl_2$	Thermo Fisher Scientific	N8080130
Glycerin	Applichem	A3739
Glycine	Applichem	A1067
Halt™ Protease Inhibitor Cocktail (100X)	Thermo Fisher Scientific	78430
Hanks' Balanced Salt Solution (HBSS)	Thermo Fisher Scientific	14025092
HEPES Buffered Saline Solution (HBSS)	Lonza	CC-5024
Hydrochloric acid (HCl) 37%	Roth	9277.1
Light Cycler 480 Sybr Green I Master	Roche	04 887 352 001
Lipofectamine® 2000 Transfection Reagent	Thermo Fisher Scientific	11668-019
Mammalian Protein Extraction Reagent (M-PER™)	Thermo Fisher Scientific	78501
Methanol	Merck	67-56-1
Milk powder	Roth	T145.2
MuLV Reverse Transcriptase (50 U)	Thermo Fisher Scientific	N8080018
Nonidet® P40	Applichem	A1694
Opti-MEM®	Thermo Fisher Scientific	31985-070
Paraformaldehyde powder (PFA)	Sigma-Aldrich	158127
PCR Nucleotide Mix 10 mM	Promega	C1141
Phosphate-Buffered Saline (PBS)	Thermo Fisher Scientific	10010031
Protein Marker V	Peqlab	27-2211
QIAzol Lysis Reagent	Qiagen	79306
Random Hexamers (50 µM)	Thermo Fisher Scientific	N8080127
Recombinant Human TGF-beta 1 Protein	R&D Systems	240-B-010
Restore™ PLUS Western Blot Stripping Buffer	Thermo Fisher Scientific	46430

RNase inhibitor	Thermo Fisher Scientific	N8080119
ROTIPHORESE®-Acrylamid-Bisacrylamid	Roth	3029.1
SDS Pellets	Roth	CN30.1
Sodium Chloride (NaCl)	Thermo Fisher Scientific	AM9759
Sodium deoxycholate monohydrate	Alfa Aesar	B20759
TaqMan® Universal Master Mix II	Thermo Fisher Scientific	4440048
TEMED	Thermo Fisher Scientific	17919
Thapsigargin, 5 mg	Santa Cruz	sc-24017A
Tris for buffer solutions	Applichem	A1379
Triton® X-100	Applichem	A4975
Trypan Blue	Sigma-Aldrich	T8154
TrypLE™ Express Enzyme	Thermo Fisher Scientific	12605-010
Trypsin / EDTA	Lonza	CC-5012
Trypsin neutralizing solution	Lonza	CC-5002
Tunicamycin from Streptomyces species	Sigma-Aldrich	T7765-5MG
Tween® 20	Applichem	A4974
UltraPure™ DNase / RNase-Free Distilled Water	Thermo Fisher Scientific	10977035
Xylene	Applichem	141769

TABLE 4: KITS

Product	Manufacturer	Cat#
BrdU Cell Proliferation Assay Kit	Cell Signalling Technology	6813
Pierce™ BCA Protein Assay Kit	Thermo Fisher Scientific	23225
Power SYBR® Green RNA-to-CT™ 1-Step Kit	Thermo Fisher Scientific	4389986
Sircol™ Collagen Assay Standard Kit	Biocolor	S1000
TaqMan® MicroRNA Reverse Transcription Kit	Thermo Fisher Scientific	4366597
Total RNA Kit, peqGOLD	Peqlab	12-6834-02

3.1.3 CELLS

TABLE 5: CELLS

Product	Manufacturer	Cat#
Primary human bronchial epithelial cells	Lonza	CC-2540

3.1.4 MEDIA

TABLE 6: MEDIA

Product	Manufacturer	Cat#
BEBM Basal Medium 500 ml	Lonza	CC-3171
+ BEGM SingleQuot Kit Suppl. & Growth Factors	Lonza	CC-4175
+ Penicillin / streptomycin (10,000 U/ml)	Thermo Fisher Scientific	15140-122
DMEM / F-12, HEPES	Thermo Fisher Scientific	31330
+ 20% FBS Sera Plus	Pan Biotech	P-303702
+ 100 units penicillin / streptomycin	Life Technologies	15140
PneumaCult™-ALI Medium	Stemcell Technologies	05001

3.1.5 CONSUMABLES

TABLE 7: CONSUMABLES

Product	Manufacturer	Cat#
100 mm TC-Treated Culture Dish	Corning	430167
12 mm Transwell® with 0.4 µm Pore Polyester Membrane Insert	Corning	3460
384 Well PCR Plate	Phenix Research Products	MPS-3898
96-well plate	Phenix Research Products	MPC-3420
96-well plate	Sigma-Aldrich	CLS3595
Cell Scraper 25 mm	Sarstedt	83.1830
Eppendorf® LoBind microcentrifuge tubes	Sigma-Aldrich	Z666505
Falcon® 6 Well Cell Culture Plate	Corning	353046
Falcon™ 15 mL Tube	Thermo Fisher Scientific	14-959-53A
Glass plate	VWR	631-1365
Immobilon-P Membran, PVDF	Merck	IPVH00010
Light Cycler 480 Multiwell plate 96	Kisker	GK480K-100
Menzel™ Microscope Coverslips	Fisher Scientific	11911998
Mini-PROTEAN® TGX™ Precast Protein Gels	BioRad	4561084
Safe-Lock Tube, 1.5 ml	Eppendorf	0030120086

Safe-Lock Tube, 2 ml	Eppendorf	0030120094
SafeSeal-Tips Premium	Biozym	692139X
SuperFrost Plus™ Adhesion slides	Thermo Scientific	10149870
T-25 flask	Corning	353109
Ultra Clear RT-PCR film	Kisker	GK480-OS

3.1.6 PRIMER

TABLE 8: MRNA PRIMER

Product	Species	Manufacturer	Sequence
CRTAP forward	Human	Eurofins Genomics	ATTATAAGTTGAACGACCTGA
CRTAP reverse	Human	Eurofins Genomics	TGTGGTACTGGTAATACACC
DHX-8 forward	Human	Eurofins Genomics	TGACCCAGAGAAGTGGGAGA
DHX-8 reverse	Human	Eurofins Genomics	ATCTCAAGGTCCTCATCTTCTTCA
HMBS forward	Human	Eurofins Genomics	TGGGCAACTGTACCTGACTG
HMBS reverse	Human	Eurofins Genomics	AGTGATGCCTACCAACTGTGG
HPRT forward	Human	Eurofins Genomics	AAGGACCCCACGAAGTGTTG
HPRT reverse	Human	Eurofins Genomics	GGCTTTGTATTTTGCTTTTCCA
P3H1 forward	Human	Eurofins Genomics	AAGCTGCTGACCACACT
P3H1 reverse	Human	Eurofins Genomics	GCAGATCAGGCGTCA
P3H2 forward	Human	Eurofins Genomics	GCTTACACATTTCGAGACTA
P3H2 reverse	Human	Eurofins Genomics	ATAGAGGCAGTCACAGTCTT
p63 forward	Human	Eurofins Genomics	CCCGTTTCGTCAGAACACAC
p63 reverse	Human	Eurofins Genomics	CATAAGTCTCACGGCCCCTC

TABLE 9: MICRORNA PRIMER

Product	Manufacturer	Cat# / Assay ID	Sequence
miR-29b	Thermo Fisher Scientific	4427975 / 000413	UAGCACCAUUUGAAAUCAGUGUU
RNU43	Thermo Fisher Scientific	4427975 / 001095	GAACTTATTGACGGGCGGACAGAA-ACTGTGTGCTGATTGTCACGTTCTGATT

3.1.7 siRNA and microRNA

TABLE 10: SIRNA TRANSFECTION REAGENTS

Product	Gene alias	Cat#	siRNA ID	Manufacturer
CRTAP	CRTAP	4392420	s20559	Thermo Fisher Scientific
LEPRE1	P3H1	4392420	s34536	Thermo Fisher Scientific
LEPREL1	P3H2	4392420	s230281	Thermo Fisher Scientific
Negative control	-	AM4611	n/s	Thermo Fisher Scientific

TABLE 11: MICRORNA TRANSFECTION REAGENTS

Product	Cat#	Assay ID	Manufacturer
miRNA29b-inhibitor	AM17000	AM10103	Thermo Fisher Scientific
miRNA29b-precursor	AM17100	PM10103	Thermo Fisher Scientific
Pre-miR Negative Control	AM17121	n/s	Thermo Fisher Scientific

3.1.8 Antibodies

TABLE 12: PRIMARY ANTIBODIES FOR WESTERN BLOT

Product	Host	Manufacturer	Cat#	Dilution (Diluent)
ß-Actin-HRP	Mouse	Sigma-Aldrich	A3854	1:100,000 (5% BSA in TBS-T)
BiP	Rabbit	Cell Signaling	3177 (C50B12)	1:1000 (5% milk in TBS-T)
CRTAP	Rabbit	Sigma-Aldrich	HPA043598	1:1000 (5% BSA in TBS-T)
GAPDH-HRP	Rabbit	Cell Signaling	3683 (14C10)	1:1000 (1% milk in TBS-T)
Krt5	Rabbit	Abcam	ab52635	1:1000 (5% BSA in TBS-T)
P3H1	Rabbit	Sigma-Aldrich	HPA012113	1:1000 (5% BSA in TBS-T)
P3H2	Rabbit	Sigma-Aldrich	HPA007890	1:1000 (5% BSA in TBS-T)
p63	Rabbit	Abcam	ab124762	1:1000 (5% BSA in TBS-T)
PCNA	Mouse	Thermo Fisher	180110	1:1000 (5% BSA in TBS-T)
Phospho-SMAD3	Rabbit	Abcam	ab52903	1:1000 (5% BSA in TBS-T)
Total-SMAD3	Rabbit	Abcam	ab28379	1:1000 (5% BSA in TBS-T)

TABLE 13: SECONDARY ANTIBODIES FOR WESTERN BLOT

Product	Manufacturer	Cat#	Dilution (Diluent)
ECL Mouse IgG, HRP-linked (from sheep)	GE Healthcare	NA931	1:60,000 (1% milk in TBS-T)
ECL Rabbit IgG, HRP-linked (from donkey)	GE Healthcare	NA934	1:60,000 (1% milk in TBS-T)

TABLE 14: PRIMARY ANTIBODIES FOR IF-STAINING OF LUNG TISSUE (LT) AND TRANSWELL MEMBRANES (TM)

Product	Host	Manufacturer	Cat#	Dilution
αSMA	Mouse	Sigma-Aldrich	A5228	1:100 (LT)
acTub	Mouse	Sigma-Aldrich	T7451	1:200 (LT)
acTub	Rabbit	Abcam	ab125356	1:500 (TM)
CC10	Mouse	Santa Cruz	sc-365992	1:100 (LT)
CC10	Rabbit	Santa Cruz	sc-25554	1:300 (TM)
KRT14	Mouse	Abcam	ab7800	1:100 (LT)
Muc5AC	Mouse	Abcam	ab3649	1:250 (TM)
P3H1	Rabbit	Sigma-Aldrich	HPA012113	1:100 (LT)
p63	Mouse	Santa Cruz	sc-8431	1:10 (LT)

TABLE 15: SECONDARY ANTIBODIES FOR IF-STAINING OF LUNGE TISSUE (LT) AND TRANSWELL MEMBRANES (TM)

Product	Manufacturer	Cat#	Dilution
Donkey anti-Mouse IgG (H+L), Alexa Fluor® 488 conjugate (green)	Thermo Fisher Scientific	A-21202	1:250 (LT) 1:400 (TM)
Donkey anti-Rabbit IgG (H+L), Alexa Fluor® 568 conjugate (red)	Thermo Fisher Scientific	A10042	1:250 (LT) 1:400 (TM)

3.1.9 BUFFERS AND RECIPES

TABLE 16: BUFFERS AND RECIPES

Product	Compound	Volume / Concentration
Lämmli buffer 6X	Tris	375 mM
	DTT	600 mM
	SDS	12%
	HCl	*Adjust pH to 6.8*
	Gycerol	60%
	Bromophenolblue	0.06%
Radio-immunoprecipitation assay	Tris	250 mM
(RIPA) buffer 5X	ddH_2O	50 ml
	HCl	*Adjust pH to 8.0*
	NaCl	750 mM
	Sodium deoxycholate	2.5%
	NP-40	5%
	SDS	0.5%
Running buffer 10X	Tris	250 mM
	Glycine	1.92 M
	SDS	1%
	MilliQ H_2O	*Adjust volume to 2 l*
TBS 10X	NaCl	160 g
	Tris	48.4 g
	MilliQ H_2O	*Dissolve in 1.5 l*
	HCl	*Adjust pH to 7.6*
	MilliQ H_2O	*Adjust volume to 2 l*
TBS 1X	10X TBS	100 ml
	MilliQ H_2O	900 ml
TBS-T 1X	10X TBS	100 ml
	MilliQ H_2O	900 ml
	Tween20	1 ml
Transfer buffer 1X	Tris	11.65 g
	Glycine	59.5 g
	SDS	0.55 g

	Methanol	200 ml
	MilliQ H_2O	*Adjust volume to 2 l*
Tris buffer pH 6.8	Tris	0.5 M
	MilliQ H_2O	*Adjust volume to 450 ml*
	HCl	*Adjust pH to 6.8*
	MilliQ H_2O	*Adjust volume to 500 ml*
Tris buffer pH 8.8	Tris	1.5 M
	MilliQ H_2O	*Adjust volume to 900 ml*
	HCl	*Adjust pH to 8.8*
	MilliQ H_2O	*Adjust volume to 1 l*
Western blot resolving gel (10%)	ddH_2O	4 ml
	1.5 M Tris buffer, pH 8.8	2.5 ml
	10% SDS	100 µl
	30% Acryl-Bisacrylamide mix	3.34 ml
	Temed	8 µl
	10% Ammonium Persulfate	50 µl
Western blot stacking gel (4%)	ddH_2O	3.01 ml
	0.5 M Tris buffer pH 6.8	1.25 ml
	10% SDS	50 µl
	30% Acryl-Bisacrylamide mix	0.66 ml
	Temed	4 µl
	10% Ammonium Persulfate	25 µl

3.2 METHODS

3.2.1 BIOBANK AND ETHICAL GUIDELINES FOR HUMAN SAMPLE RETRIEVAL

All analyzed human specimens were obtained from the BioArchive CPC-M at the Comprehensive Pneumology Center (CPC) in Munich, Germany and the Lung tissue research consortium (LTRC) biobank at Yale University in New Haven, United States of America. Lung explant material from IPF patients was characterized regarding known IPF features of usual interstitial pneumonia (UIP), as described by Staab-Weijnitz et al. in 2015.[44] Patients agreed in a written statement on the use of their lung tissue for comprehensive research and its use was approved by local ethics committees according to effective guidelines (454-12 [CPC-M], 1601017047 [LTRC]).

3.2.2 CELL CULTURE

3.2.2.1 PRIMARY HUMAN LUNG FIBROBLASTS

Primary human lung fibroblasts (phLF) from the BioArchive CPC-M were expanded in DMEM / F-12 with FBS and pen / strep in standard conditions at 37 °C, 95% air humidity and 5% CO_2. The medium was changed every other day until the cells reached 90-100% confluence. The phLF monolayer was washed with DPBS following cell detachment using 2 ml TrypLE Express Enzyme per dish. 8 ml medium was added and the cell suspensions from three dishes were pooled. For subsequent experiments, 21,000 passage 10 phLF per cm^2 were seeded and grown to 90-100% confluence.

3.2.2.2 PRIMARY HUMAN BRONCHIAL EPITHELIAL CELLS

For *in vitro* experiments with undifferentiated basal-like or differentiated bronchial epithelial cells, normal primary human bronchial epithelial cells (pHBECs) were used from four different healthy donors.

Initially, one vial containing 500,000 passage 0 pHBECs was thawed from -160 °C and transferred to a 15 ml Falcon Tube containing 4.5 ml of warm BEGM including supplements and antibiotics. The pHBECs were distributed to 6 T-25 flasks containing 5 ml of pre-warmed BEGM each and incubated in standard conditions. After 24 hours, the BEGM was changed to remove DMSO residues and thereafter changed every other day. After 5-6 days, pHBECs reached 80% confluence and a cell count of roughly 1 million per flask.

The following steps were performed for storage and re-expansion of passage 1 pHBECs. After the initial passage 0 expansion as described above, the medium was aspirated and the pHBEC-monolayer was washed with 5 ml HBSS. The pHBEC monolayer was covered with 2 ml Trypsin / EDTA and incubated at 37 °C for five to ten minutes. Detachment of pHBECs was monitored under the light microscope and gently supported by tapping. 4 ml trypsin neutralizing solution was added to each flask. The pooled pHBEC cell suspension was centrifuged with 300 × g for five minutes, supernatant medium was aspirated and the cell-pellet was re-suspended in 6 ml BEGM including 20% FBS. 20 µl of cell suspension were mixed with 20 µl Trypan Blue and counted in a Newbauer chamber. 500,000 pHBECs were added to 6 ml warm BEGM and distributed to 6 T-25 flasks as described above for re-expansion and experimental use in passage 1. Remaining pHBECs were stored in 500,000 cells per

vial after adding 10% DMSO to the cell suspension in BEGM / FBS. The vials were cooled down gradually to the final storage temperature at -160 °C.

3.2.2.3 pHBEC DIFFERENTIATION AT THE AIR-LIQUID-INTERFACE

The Air-Liquid-Interface (ALI) model allows the differentiation of pHBECs into a mucociliary epithelium, containing CC10-positive Clara cells, acTub-positive ciliated cells and Muc5AC- and Muc5B-positive goblet cells on top of remaining p63- and Krt14-positive basal-like cells.[45]

After expanding passage 1 pHBECs in BEGM for 5-6 days, cells were harvested and seeded on a Transwell Membrane Insert in a density of 90,000-100,000 per cm^2 (Figure 1, **A**). Both the apical and the basolateral compartment were filled with 0.5 ml and 1 ml BEGM, respectively. After the cell layer reached 100% confluence, the apical medium was removed and 1 ml ALI-Medium replaced the BEGM in the basolateral compartment (Figure 1, **B**). The cells were fully differentiated circa 28 days after "airlift" in ALI-culture (Figure 1, **C**).[45] To remove mucus, the apical surface was washed with HBSS weekly after airlift and ALI-medium was changed every other day.

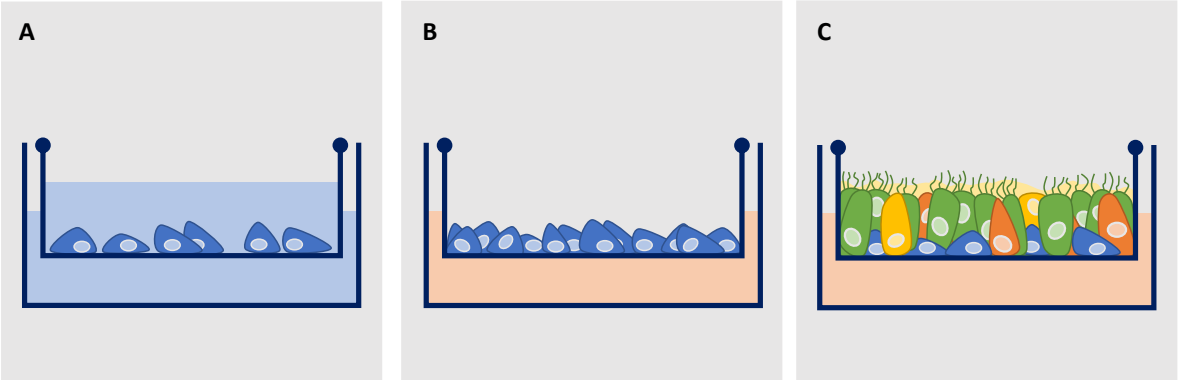

FIGURE 1: *IN VITRO* DIFFERENTIATION OF PRIMARY HUMAN BRONCHIAL EPITHELIAL CELLS INTO A MUCOCILIARY EPITHELIUM. (**A**) SHOWING EXPANSION PHASE OF PHBECS ON A SEMIPERMEABLE TRANSWELL MEMBRANE IN SUBMERGED CULTURE USING BEGM. (**B**) "AIRLIFTING" OF FULLY CONFLUENT PHEBCS AFTER ONE WEEK IN SUBMERGED CULTURE. REPLACEMENT OF BEGM WITH ALI CULTURING MEDIUM IN BASOLATERAL COMPARTMENT, EXPOSURE TO HUMIDIFIED AIR ON APICAL COMPARTMENT. (**C**) MUCOCILIARY AIRWAY EPITHELIUM AFTER THE FOUR WEEK DIFFERENTIATION PHASE ON AIR-LIQUID-INTERFACE. BASAL-LIKE CELLS SHOWN IN BLUE, CILIATED CELLS SHOWN IN GREEN, GOLBET CELLS AND MUCUS SHOWN IN YELLOW, CLARA CELLS SHOWN IN ORANGE.

3.2.2.4 siRNA-transfection

Gene knockdown experiments were performed using pre-designed double-stranded silencer RNA (siRNA) in a final concentration of 2, 10 and 30 nM and lipofectamine 2000 transfection reagent according to the manufacturer's instructions. Lipofectamine and the respective siRNA were incubated in Opti-MEM at room temperature for 20 minutes. The transfection reagents were then mixed with cell culture medium and applied to phLF or pHBECs. After 24 hours, the transfection solution was aspirated and replaced by either regular medium or further treatment solutions.

Reverse transfection experiments were performed immediately when the cells were seeded into culture vessels. Forward transfection was performed on 80-90% confluent cells.

3.2.2.5 Treatment with microRNA29b-inhibitor and -precursor

pHBECs in passage 2 were treated with a microRNA29b-inhibitor and –precursor as well as scrambled microRNA in 6-well plates at 80% confluence. 24 hours prior to the transfection, the culture medium was replaced by antibiotics-free BEGM without both the gentamycin aliquot from the Bullet Kit and pen / strep. 5 µl lipofectamine and 5 µl of the respective treatment reagent per 6-well were diluted in 250 µl Opti-MEM each and incubated separately for 5 minutes at room temperature. Opti-MEM with lipofectamine was combined with the treatment containing Opti-MEM mixture and incubated for 15 minutes at room temperature. Growth media were aspirated from the pHBECs and 2 ml BEGM without antibiotics were added to each well together with 500 µl of the individual treatment solutions to a final concentration of 100 nM for miR29b-inhibitor, -precursor and scrambled negative control. 6 hours after treatment application, the transfection medium was replaced with BEGM including antibiotics.

3.2.2.6 Treatment with TGFß-1

For *in vitro* stimulation with Transforming Growth Factor β-1 (TGFβ-1), phLF or pHBEC culturing media were prepared with 0.1 mM ascorbate. Recombinant human TGFβ-1 was added to a final concentration of 1 or 2 ng/ml in ascorbate substituted media. Control media without TGFβ-1 were also substituted with ascorbate.

3.2.2.7 TREATMENT WITH TUNICAMYCIN AND THAPSIGARGIN

10,000 passage 2 pHBECs per cm^2 were expanded in BEGM. The cells were subsequently challenged with endoplasmic reticulum (ER) stress for 24 and 48 hours using the glycosylation inhibitor tunicamycin and the sarcoplasmic / endoplasmic reticulum Ca^{2+} ATPase (SERCA) inhibitor thapsigargin. Tunicamycin and thapsigargin were administered to the cells in BEGM in final concentration of 1 µM and 60 nM, respectively. Both reagents are stored in 100% DMSO. Therefore, control media were substituted with the equivalent amount of DMSO.

3.2.2.8 BRDU CELL PROLIFERATION ASSAY

To assess cell proliferation in pHBECs, the Bromdesoxyuridin (BrdU) uptake was measured using the BrdU Cell Proliferation Assay Kit according to the manufacturer's instructions. Experiments on submerged pHBECs were performed in 96-well plates in 200 µl BEGM containing treatment solutions or controls. Final color intensities were detected using the Sunrise Reader at a wavelength of 450 nm.

3.2.3 RNA ANALYSIS

3.2.3.1 RNA-EXTRACTION AND CDNA-TRANSCRIPTION

The following steps describe RNA-extraction from -80 °C shock-frozen pHBECs after experiments in submerged culture using the peqGOLD Total RNA Kit according to the manufacturer's instructions. RNA purification was performed using DNase digestion buffer. Final RNA elution was performed in 35 µl RNase free ddH_2O for three minutes and subsequent centrifugation at 5000 × g for 1 minute. RNA lysates were stored at -80 °C.

In preparation of quantitative Real-Time Polymerase Chain Reaction (qRT-PCR) analysis, the collected messenger RNA (mRNA) was reverse transcribed into complementary DNA (cDNA). Total RNA-concentrations were determined using the NanoDrop Spectrophotometer. 1 µg RNA was calculated for the individual sample and filled up to 20 µl with RNase-free ddH_2O. The samples were denatured at 70 °C for ten minutes. 20 µl of reverse transcriptase reaction mix were prepared, containing 4 µl 10X PCR Buffer II, 8 µl 25 mM $MgCl_2$, 2 µl dNTP's (10 mM each), 2 µl Random Hexamers, 1 µl RNase

Inhibitor, 2 µl MuLV Reverse Transcriptase and 1 µl RNase-free ddH_2O. The mix was added to each sample and mixed thoroughly by pipetting. The total volume of 40 µl was heated to 37 °C for 60 minutes, then to 75 °C for 10 minutes in the Light Cycler. The transcribed cDNA was diluted in 160 µl RNase free ddH_2O to a final concentration of 5 µg/ml. 12.5 ng cDNA were used for one single qPCR reaction.

3.2.3.2 PRIMERDESIGN

Reverse and forward SYBR green primers for desired target-mRNAs were selected using the NCBI primer BLAST tool at blast.ncbi.nlm.nih.gov. Primer length was determined 18-20 nucleotides, PCR product size 70-150 nucleotides and melting temperature 59-61 °C. Primer-pairs were double-checked for efficacy, hairpin formation and thermodynamic parameters using Primer3web version 4.1.0 at primer3.ut.ee.

3.2.3.3 QUANTITATIVE REAL-TIME-PCR

SYBR Green based qRT-PCR was performed to amplify and detect specific mRNA-sequences previously transcribed into cDNA using validated SYBR green primer-pairs.

Samples were placed in a white Light Cycler 480 Multiwell plate 96 in triplicates for each target and housekeeper mRNA. The total amount of cDNA per well was 12.5 ng (2.5 µl in a concentration of 5 µg/ml). 5 µl Light Cycler 480 Sybr Green I Master, 1.5 µl purified H_2O and 1 µl of the individual primer-pair-solution containing reverse and forward primers in a concentration of 10 pmol/µl each were added to each well. The plate was sealed with Ultra Clear RT-PCR film and run in the Light Cycler following the protocol stated in Table 17.

TABLE 17: LIGHT CYCLER PROTOCOL FOR SYBR GREEN BASED QRT-PCR

Process	Temperature	Time	# of cycles
Pre-Incubation	95 °C	5 min	1
Amplification	95 °C	5 sec	45
	59 °C	5 sec	
	72 °C	10 sec	
Melting curve	95 °C	5 sec	1
	60 °C	1 min	
	Steady heating until 95 °C	2 min	
	95 °C	5 sec	
Cooling	4 °C	∞	1

3.2.3.4 mRNA ANALYSIS IN MIR-STIMULATED CELLS

RNA extraction from miRNA29b-treated pHBECs was performed using the following protocol to collect small RNA species. After treatment, media were aspirated and the cell monolayer washed with 2 ml DPBS per well. 700 µl of QIAzol Lysis Reagent was distributed to the cells. The cells were scratched and the lysate was transferred to a 1.5 ml reaction tube. After a five-minute incubation time at room temperature, 140 µl chloroform were added and the tubes were mixed vigorously. The lysate was centrifuged at 12,000 × g for 15 min at 4 °C. Samples were kept on ice. After spinning, the aqueous phase (approximately 300 µl) was transferred to a new 2 ml reaction tube and placed into the QIAcube. The miRNeasy Mini Kit protocol was run with an elution volume of 40 µl. After concentration measurement with the NanoDrop Spectrophotometer, eluted total RNA lysates were stored at -80 °C.

For reverse transcription and transcript analysis, the Power SYBR® Green RNA-to-CT™ 1-Step Kit was used with the SYBR Green primer pairs for P3H1 and HPRT. RNA samples were diluted in ddH_2O to a final concentration of 5.12 ng/µl. 25ng RNA (equals 4.88 µl) per reaction were mixed with prepared primer-mastermixes containing 0.02 µl forward and 0.02 µl reverse primer (equals 10 pmol/µl each), 0.08 µl 125X RT Enzyme Mix and 5 µl 2X Power SYBR Green RT-PCR Mix provided by the Kit in a 384-Well PCR Plate. The plate was centrifuged for 2 minutes at 711 × g. The Light Cycler protocol stated in Table 18 was used for reverse transcription and qRT-PCR.

TABLE 18: LIGHT CYCLER PROTOCOL FOR 1-STEP REVERSE TRANSCRIPTION AND QRT-PCR

Process	Temperature	Time	# of cycles
Reverse Transcription	48 °C	10 min	1
Pre-Incubation	95 °C	10 min	1
Amplification	95 °C	15 sec	40
	60 °C	60 sec	
Melting curve	95 °C	5 sec	1
	60 °C	1 min	
	Steady heating until 95 °C	2 min	
	95 °C	5 sec	
Cooling	4 °C	∞	1

3.2.3.5 MICRORNA ANALYSIS IN MIR-STIMULATED CELLS

Reverse transcription and qRT-PCR of microRNAs was conducted separately. For reverse transcription of miR29b and the endogenous control RNU43, RNA samples were diluted in ddH_2O to a final concentration of 2 ng/µl. Primer mastermixes were prepared with 4 µl of 5X Mixed RT Taq-Man Primers for miR29b and RNU43 together with the reagents provided by the TaqMan® MicroRNA Reverse Transcription Kit (0.4 µl 100 mM dNTP, 2 µl Reverse Transcriptase, 2 µl 10X RT Buffer, 0.25 µl RNase Inhibitor and 1.35 µl ddH_2O). 10µl of the respective mastermix were mixed with 10 µl of 2 ng/µl RNA (equals 20 ng RNA per reaction) in a 96-Well plate, which was centrifuged for 2 minutes at 711 × g and incubated on ice for 5 minutes. The plate was run in a Thermal Cycler at 16 °C for 30 minutes, 42 °C for 30 minutes, and 85 °C for 5 minutes. 180 µl ddH_2O were added to each well to a final cDNA concentration of 0.1 ng/µl and samples were stored at -20 °C.

qRT-PCR analysis was performed using 0.8 µl cDNA per reaction, mixed with 0.5 µl 20X TaqMan Primers for miR29b and RNU43, 5 µl 2X TaqMan Universal Master Mix II and 3.7 µl ddH_2O in a 384-Well PCR plate. The plate was sealed with Ultra Clear RT-PCR film and run in the Light Cycler following the protocol stated in Table 19.

TABLE 19: LIGHT CYCLER PROTOCOL FOR QRT-PCR OF MICRO-RNA SAMPLES

Process	Temperature	Time	# of cycles
Pre-Incubation	95 °C	10 min	1
Amplification	95 °C	15 sec	40
	60 °C	60 sec	
Cooling	4 °C	∞	1

3.2.4 PROTEIN ANALYSIS

3.2.4.1 PROTEIN EXTRACTION AND CONCENTRATION DETERMINATION

phLF and pHBECs were shock-frozen in individual culture vessels at -80 °C. To harvest protein lysates, the vessels were thawed briefly and incubated with 150 µl RIPA buffer for two minutes on ice. The cells were scratched and incubated for another five minutes on ice. The cell lysate was transferred to a 1.5 ml reaction tube and incubated for 30 minutes on ice. The samples were centrifuged for 15 minutes at 15,000 × g and 4 °C. The supernatant protein lysate was collected and stored at -20 °C.

For concentration determination, the Bicinchoninic acid (BCA) assay was performed using the Pierce BCA Protein Assay Kit. Sample-triplicates were prepared in a 96-Well plate in a total volume of 10 µl. RIPA-buffer was plated in triplicates for blank measurement. Duplicates of lysates with known protein concentration ranging from 0 to 2 mg/ml were put on each plate for reference. For the colorimetric detection, the provided Pierce BCA Protein Assay Reagents A and B were mixed according to the manufacturer's instructions and 200 µl were added to each well. The plate was incubated lightproof for 30 minutes at 37 °C and read using the Sunrise Reader at a detection wavelength of 562 nm.

3.2.4.2 SDS-PAGE, WESTERN BLOT AND IMMUNOCHEMICAL PROTEIN DETECTION

SDS polyacrylamide gel electrophoresis (SDS-PAGE) was performed to separate proteins of total lung tissue homogenates and cell culture protein lysates using 10% separation gels and 4% stacking gels. Protein samples were prepared by calculating the lysate volume for 30 µg or 20 µg total protein and mixing it with H_2O and a 6X-stock concentration of Lämmli buffer to the final concentration of 1X Lämmli buffer. Samples were heated at 95 °C for five minutes and then centrifuged at 10,000 × g for

one minute. Prepared gels were placed into a Mini-PROTEAN Tetra Cell filled with 1X-running buffer. The samples were filled into the slots, as well as the Protein Marker V. Both empty and marker wells were filled with 1X Lämmli buffer to equal final volumes. The samples were run at 80 V for 80 minutes.

After SDS-PAGE, the gel was removed and rinsed with transfer buffer. The PVDF-membrane for subsequent western blotting was activated in pure methanol for 30 seconds and rinsed with transfer buffer. The western blot chamber was set up with the membrane facing the anode and the gel facing the cathode. The chamber was put on ice and filled with a mix of 80% ddH_2O, 10% methanol and 10% transfer buffer. The samples were transferred at 90 V for 90 minutes.

For immunochemical protein detection, the western blot membrane was washed in TBS-T and blocked in 5% milk in TBS-T for 1 hour at room temperature. After washing with TBS-T, the membrane was incubated overnight at 4 °C with the respective primary antibody solutions. The membrane was washed in TBS-T 3 times for 5 minutes at room temperature and incubated with the secondary antibody solution for 1 hour. After another washing step, specific protein bands were detected using chemiluminescent substrates and the ChemiDoc system powered by Image Lab software.

For the detection of further proteins, the membrane was washed in TBS-T for 5 minutes and incubated with Restore PLUS Western Blot Stripping Buffer for 5 minutes at room temperature on the shaker. The membrane was washed in TBS-T 3 times for 5 minutes, blocked in 5% milk in TBS-T for 1 hour at room temperature, and washed again. Protein detection with primary and secondary antibodies was performed as described above.

3.2.4.3 WESTERN BLOT ANALYSIS IN MIR29B TREATED CELL LYSATES

Western blot analysis in lysates from miR29b treated pHBECs was in principle performed as described above with the following set of products. 24 and 48 hours after transfection, protein lysates were harvested in 150 µl Mammalian Protein Extraction Reagent including 1% Halt Protease Inhibitor Cocktail (100X). The total protein concentration was determined as described above using the Pierce BCA Protein Assay Kit. SDS-PAGE and western blot were performed using 4–15% Mini-PROTEAN Precast Protein gels and the Trans-Blot Turbo Transfer system according to manufacturer's instructions. Immunological protein detection was conducted following the protocol above using corresponding antibodies and concentrations.

3.2.4.4 COLLAGEN DETECTION IN CELL CULTURE SUPERNATANTS

Detection of secreted collagen *in vitro* was performed using the Sircol Collagen Assay Standard Kit. 1 ml of cell culture supernatants were harvested in 1.5 ml LoBind microcentrifuge tubes in quadruplicates for each treatment and stored at -80 °C. The procedure was started by thawing the supernatants and adding 200 µl cold Isolation and Concentration Reagent provided by the kit. Reference solutions with known collagen concentrations ranging from 0 µg to 30 µg were processed equally. The mix was incubated overnight at 4 °C. The tubes were spun for 30 minutes at 18,600 × g and the supernatant was discarded. 1 ml Sircol Dye Reagent was added and the tubes were incubated for 30 minutes with gently shaking at 400 rpm in a thermomixer. The tubes were spun for 30 minutes at 18,600 × g and drained again by inverting. Unbound dye was removed without touching the pellet. 750 µl ice cold Acid-Salt Wash Reagent was added to the pellet and the tube was spun for 30 minutes at 18,600 × g. After removing the washing solution, the step was repeated. The pellet was dissolved in 250 µl of Alkali Reagent using a vortexer. For measurement, 200 µl of each sample was put into a 96-well plate and read using the Sunrise Reader at a detection wavelength of 555 nm. Collagen concentrations were calculated based on reference solutions.

3.2.5 IMAGING OF LUNG TISSUE AND CULTURED CELLS

3.2.5.1 IMMUNOFLUORESCENCE STAINING OF HUMAN LUNG TISSUE

The formaline fixed and paraffin embedded human lung tissue slices on microscope slides were provided by Daniela Dietel.

The slides were heated at 60 °C for 30 minutes and the tissue was deparaffinated in xylene for 5 minutes twice. Rehydration was performed in 100% ethanol twice for 2 minutes, then one minute each in 90%, 80% and 70% ethanol and lastly in ddH_2O. After washing with 1X TRIS-buffer, the tissue was blocked with 100 µl 5% BSA in PBS for 30 minutes and washed again. 100 µl of the primary antibody solution (dilution in 5% BSA in PBS) were prepared in the appropriate concentration and applied to the tissue overnight at 4 °C in a wet chamber. After 12 hours, the slides were washed with 1X TRIS-buffer and the secondary antibody was applied to the tissue in 5% BSA in PBS together with DAPI in the final concentration of 0.5 µg/ml. The slides were incubated lightproof for 1 hour at room

temperature. After washing, the slides were covered with fluorescent mounting medium and a glass plate. The slides were stored in darkness at room temperature.

Immunofluorescent images were obtained from the Axio Imager 2.

3.2.5.2 IMMUNOFLOURESCENCE STAINING OF PHBECS CULTURED ON TRANSWELL MEMBRANES

ALI-cultured pHBECs were washed twice in HBSS and fixed with 3.7% paraformaldehyde (PFA) for 1 hour at room temperature. PFA was aspirated and the cells were stored in HBSS at 4 °C.

For IF-staining of the apical cell layer, the cells were permeabilized with 0.2% Triton X-100 / HBSS apical and basolateral for five minutes at room temperature. After washing with HBSS, unspecific binding sites were blocked with 5% BSA in TBS-T for one hour at room temperature. The membrane was cut out from the transwell insert and the primary antibody was applied in 150 µl 5% BSA / 0.2% Tween / HBSS in respective dilutions for 1 hour at room temperature on the shaker. After washing three times in HBSS, the secondary antibody was incubated in 150 µl 5% BSA / 0.2% Tween / DPBS in the appropriate dilutions for 30 minutes at room temperature. DAPI staining was applied to the secondary antibody solution in 1:1000 dilution. A final washing step was performed with HBSS. Ultimately, the membrane was placed on a microscope slide in anti-fade-medium and covered with a cover slip. The slides were stored in darkness at room temperature.

Immunofluorescent images were obtained from the Axio Imager 2.

4 RESULTS

4.1 REVERSE KNOCKDOWN OF P3H1, P3H2 AND CRTAP IN PHLF CONFIRMS ANTIBODY AND SIRNA-SPECIFICITY

To determine specificity of antibodies and silencer RNAs, primary human lung fibroblasts (phLF) were transfected with P3H1, P3H2 and CRTAP siRNA and scrambled siRNA as controls in three different concentrations (2, 10 and 30 nM). Cell lysates were analyzed by western blotting after 24 and 48 hours.

Transfection with P3H1 siRNA resulted in decrease of P3H1 protein levels after 24 hours with 2 nM and 10 nM siRNA concentration and after 48 hours for all siRNA concentrations (Figure 2, **A**). Consistent P3H2 silencing was achieved both after 24 hours and 48 hours (Figure 2, **B**). In addition to the canonical 100 kDa protein, another protein band at approximately 70 kDa was detected by the P3H2 antibody, which was downregulated after 48 hours. CRTAP protein expression was lower in

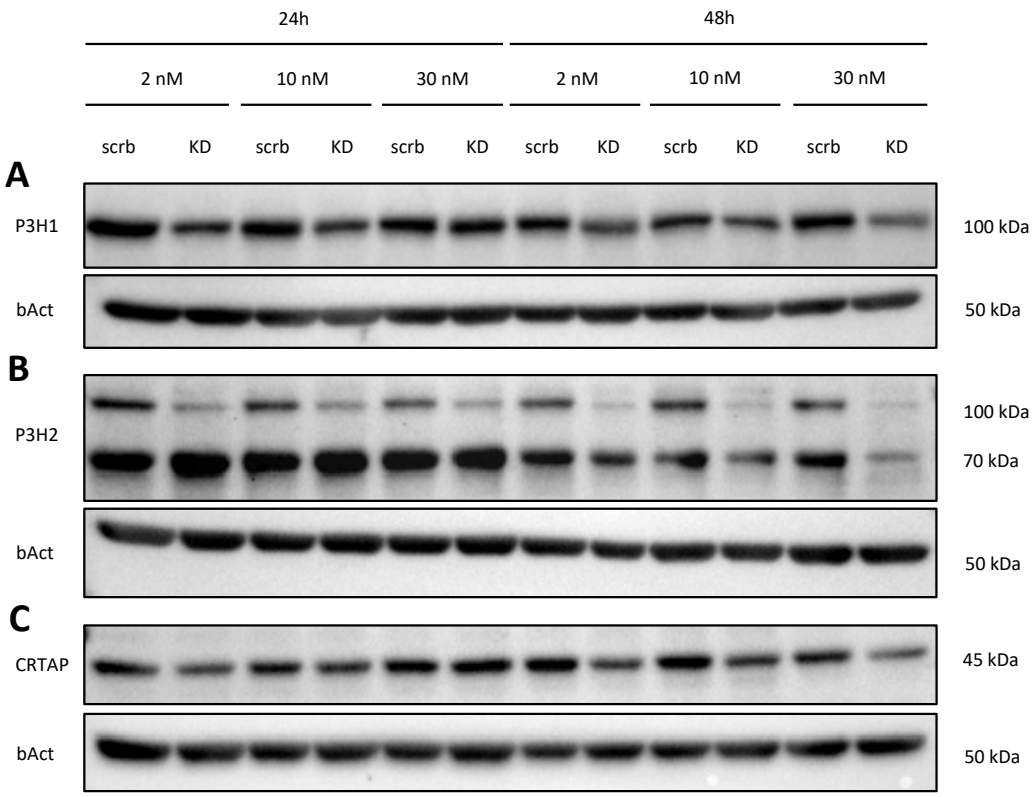

FIGURE 2: ANTIBODY AND SILENCER-RNA EVALUATION IN PHLF. (**A**) WESTERN BLOT ANALYSIS OF P3H1 AND BACT HOUSEKEEPER IN PAIRS OF SCRAMBLED CONTROL (SCRB) AND KNOCKDOWN (KD). (**B**) P3H2. (**C**) CRTAP.

siRNA transfected cells after 24 and 48 hours, except for the 30 nM concentration after 24 hours (Figure 2, **C**).

4.2 P3H1 AS WELL AS A P3H2-VARIANT ARE UPREGULATED IN IPF TOTAL LUNG HOMOGENATES

Five healthy control (HC) and six IPF total lung homogenates from the BioArchive CPC-M were analyzed for P3H1, P3H2 and CRTAP expression, as well as four HC and IPF homogenates from the lung tissue research consortium (LTRC) biobank at Yale University in the United States for P3H1 expression.

P3H1 protein levels were significantly increased in IPF samples from both the CPC-M and LTRC cohort compared to HC (Figure 3, **A**, **D**-**F**). The analysis of P3H2 did not show differential expression of the 100 kDa protein variant, but the previously documented 70 kDa band was upregulated in IPF samples (Figure 3, **B**). CRTAP was not expressed differently in the CPC-M cohort (Figure 3, **C**). Notably, there was considerable variability of all analyzed proteins within the HC and IPF subgroup.

Looking at the corresponding messenger RNAs, qRT-PCR analysis of CPC-M lung lysates did not show expression differences of neither P3H1 nor CRTAP in IPF versus HC (Figure 3, **G**, **J**). P3H2 was significantly downregulated in the CPC-M IPF samples compared to HC (Figure 3, **H**).

4.3 P3H1 IS PRESENT IN P63-POSITIVE BASAL CELLS IN IPF

4.3.1 CO-STAININGS WITH LUNG CELL MARKERS DISPLAY P3H1 TO BE PRESENT IN P63- AND KRT14-POSITIVE BASAL CELLS IN IPF TISSUE

Immunofluorescence stainings of formaline fixed paraffine embedded human HC and IPF tissue from the BioArchive CPC-M were performed to characterize P3H1 expression *in situ*.

α-Smooth-Muscle-Actin (αSMA), a commonly used marker for myofibroblasts, did not overlap with P3H1 expression in IPF tissue (Figure 4, **A**). Whereas αSMA-positive cells dominated in interstitial

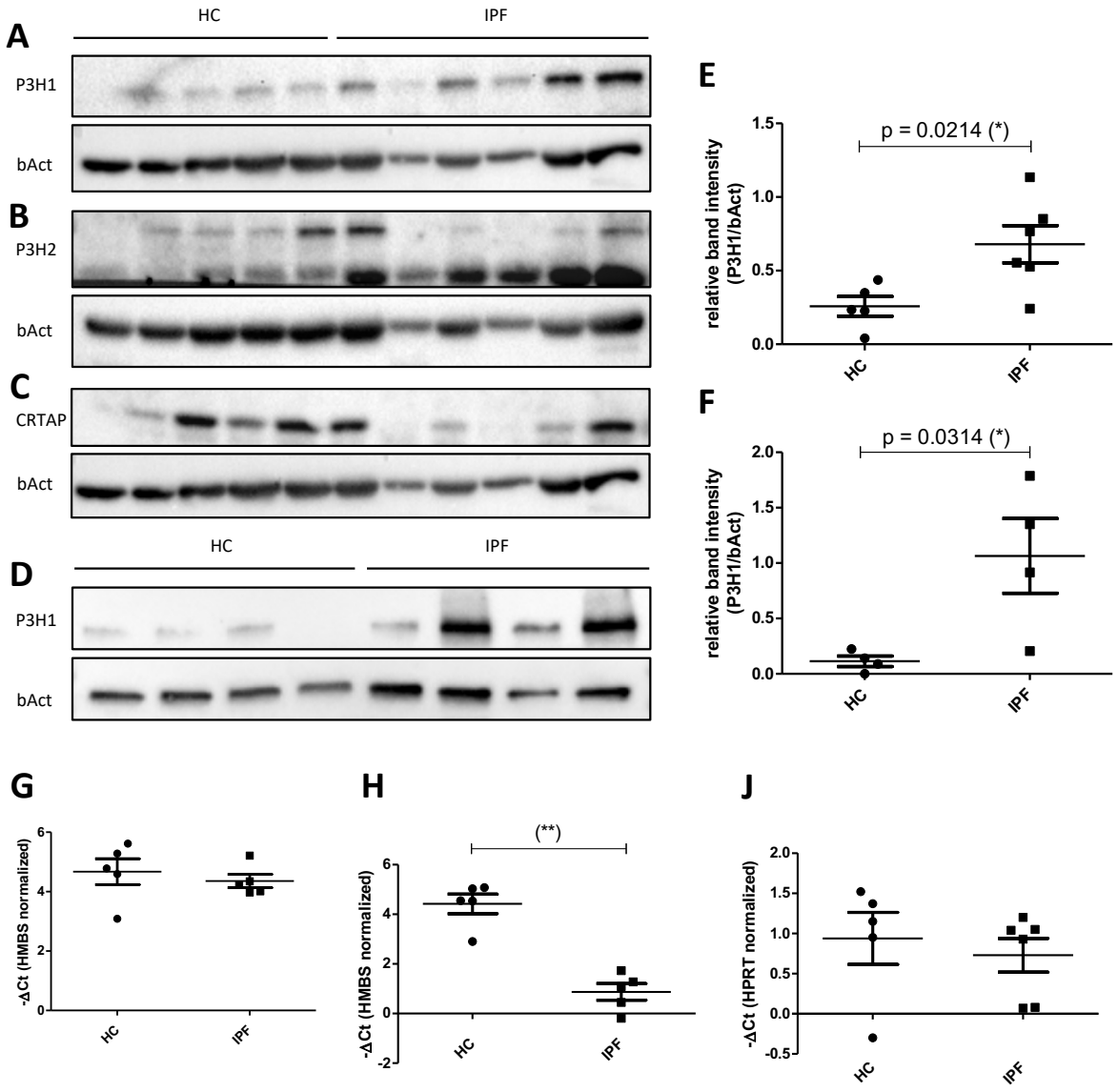

FIGURE 3: COLLAGEN HYDROXYLASES IN IPF. (A-C) WESTERN BLOT ANALYSIS OF HEALTHY CONTROL (HC, N = 5) AND IPF (N = 6) TOTAL LUNG LYSATES OF CPC-M COHORT. (**D**) HC (N = 4) AND IPF (N = 4) TOTAL LUNG LYSATES OF LTRC COHORT. (**E**, **F**) GRAPHIC PRESENTATION OF RELATIVE P3H1 BAND INTENSITY IN CPC-M COHORT (E) AND LTRC COHORT (F), (**G-J**) TRANSCRIPT EXPRESSION OF P3H1 (G), P3H2 (H) AND CRTAP (J) IN CPC-M COHORT, DATA IS PRESENTED AS -ΔCT, NORMALIZED TO HMBS (G, H) AND HPRT (J). MEAN ± SEM. STATISTICAL ANALYSIS WAS PERFORMED USING AN UN-PAIRED TWO-TAILED T-TEST. ASTERISK (*) INDICATING $P < 0.05$, (**) $P < 0.01$.

fibrotic foci and around small blood vessels, there was only faint staining of P3H1 in these lung compartments. However, in some areas around what presumably displayed as small bronchi, there were numerous pyramid-shaped cells strongly positive for P3H1. In fact, P3H1 expression in these areas exceeded P3H1 expression in healthy control tissue stained and imaged in the same conditions (Figure 4, **B, C**). To further investigate the P3H1-expressing cell type, co-stainings were performed on

serial cuts of HC and IPF tissue using established markers of bronchial epithelial cells, such as CC10 for Clara cells, acTub for ciliated cells, and Krt14 and p63 for basal cells.[45] Staining for P3H1 as well as Krt14 was overall weak in HC tissue, whereas CC10, acTub and p63 staining displayed strongly positive cells along the bronchial epithelial lining (Figure 5, **B**). In IPF, areas with this particular configuration were detected as well ($CC10^+$, $acTub^+$ and $p63^+$ cells, absence of $Krt14^+$ / $P3H1^+$ cells), but additionally, areas with strong P3H1 expression, co-localizing with $p63^+$ / $Krt14^+$ cells and complete absence of the specialized bronchial epithelial markers, suggest the presence of a second type of bronchial epithelium in IPF tissue, mainly featuring basal cells with a distinct protein expression pattern (Figure 5, **A, C**).

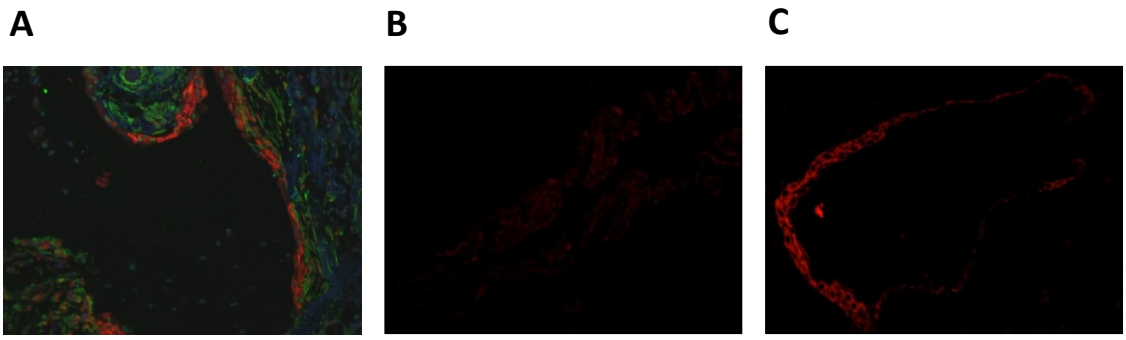

FIGURE 4: IF-STAININGS OF IPF AND HC TISSUE. (**A**) IPF INTERSTITIUM AND SMALL BRONCHUS STAINED FOR αSMA (GREEN), P3H1 (RED) AND DAPI (BLUE). (**B, C**) P3H1 STAINING (RED) IN A HC (B) AND IPF (C) SAMPLE USING IDENTICAL STAINING AND IMAGING CONDITIONS.

4.3.2 P3H1 EXPRESSION DECREASES DURING PHBEC DIFFERENTIATION INTO SPECIALIZED BRONCHIAL EPITHELIUM *IN VITRO*

P3H1 and p63 expression was assessed in differentiating bronchial epithelial cells *in vitro.* pHBECs were cultured and differentiated on the Air-Liquid-Interface for four weeks and cell lysates were evaluated for P3H1, Krt5 and p63 at day 7, 14, 21 and 28. Simultaneous membrane stainings showed increasing numbers of $Muc5AC^+$, $CC10^+$ and $acTub^+$ cells confirming successful pHBEC differentiation into goblet, clara and ciliated cells (Figure 6, **A-C**). In obtained protein lysates, decreasing p63 and Krt5 levels accordingly suggest a relative drop of undifferentiated bronchial epithelial cell count over the four-week differentiation period (Figure 6, **D**). P3H1 protein and transcript expression decreases steadily as well, which may indicate, that pHBECs are the major P3H1 expressing cell type among the bronchial epithelial cell entities (Figure 6, **D-F**).

Protein and RNA lysates from two out of three analyzed pHBEC differentiations were provided by Andrea Schamberger.

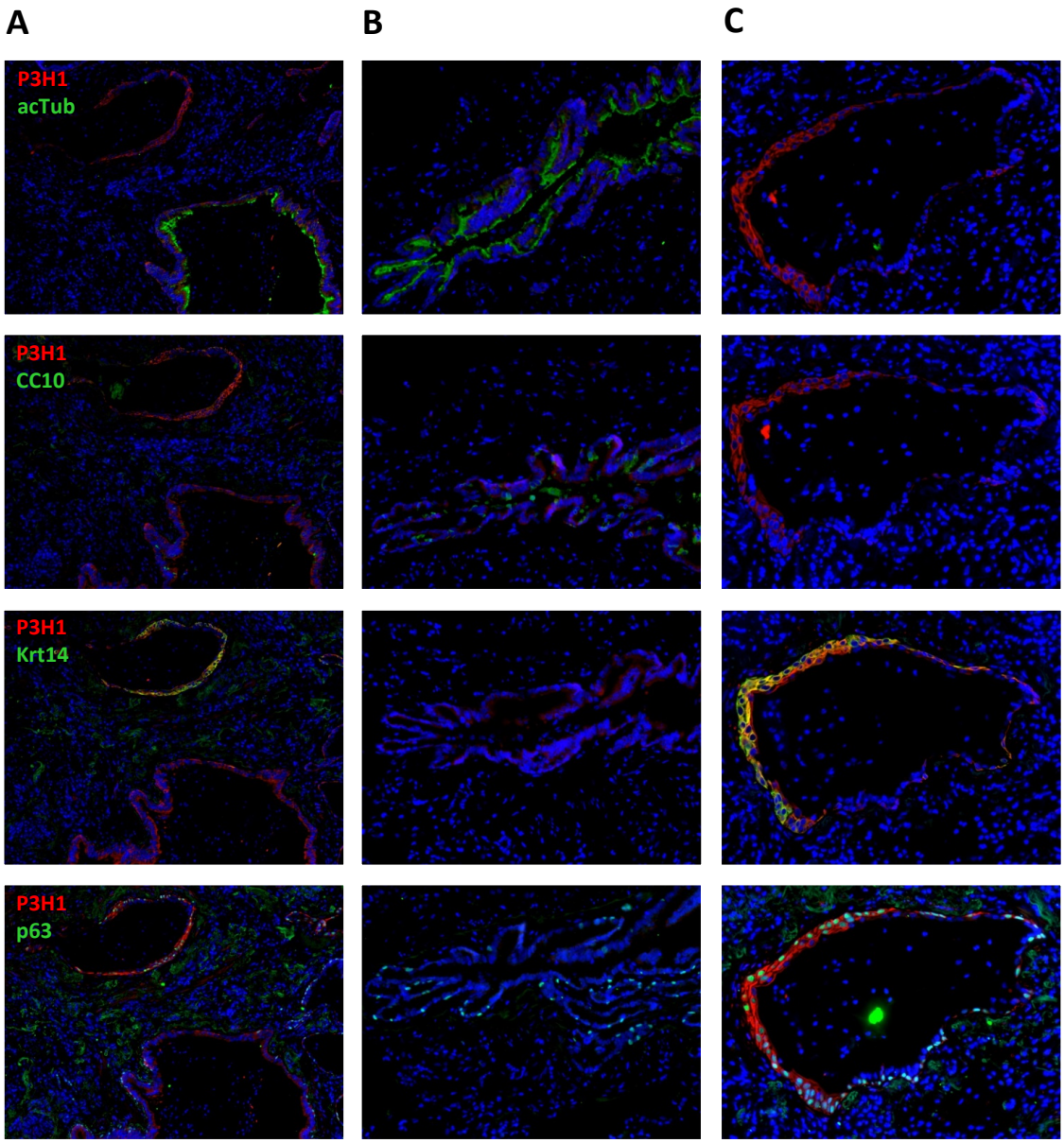

FIGURE 5: IF-STAININGS IN SERIAL CUTS OF IPF AND HC LUNG TISSUE. (COLUMN **A**) 10X MAGNIFICATION OVERVIEW OF REPRESENTATIVE IPF SECTION INCLUDING CYSTIC STRUCTURE ON TOP LEFT AND SMALL BRONCHUS ON BOTTOM RIGHT SIDE. (**B**) HC IN 20X MAGNIFICATON FEATURING A SMALL BRONCHUS. (**C**) IPF IN 20X MAGNIFICATION SHOWING A CYSTIC STRUCTURE AS SEEN IN (A). DAPI (BLUE) AND P3H1 (RED) CO-STAININGS SHOWN WITH ACTUB (GREEN) IN FIRST ROW, CC10 (GREEN) IN SECOND, KRT14 (GREEN) IN THIRD AND P63 (GREEN) IN FOURTH.

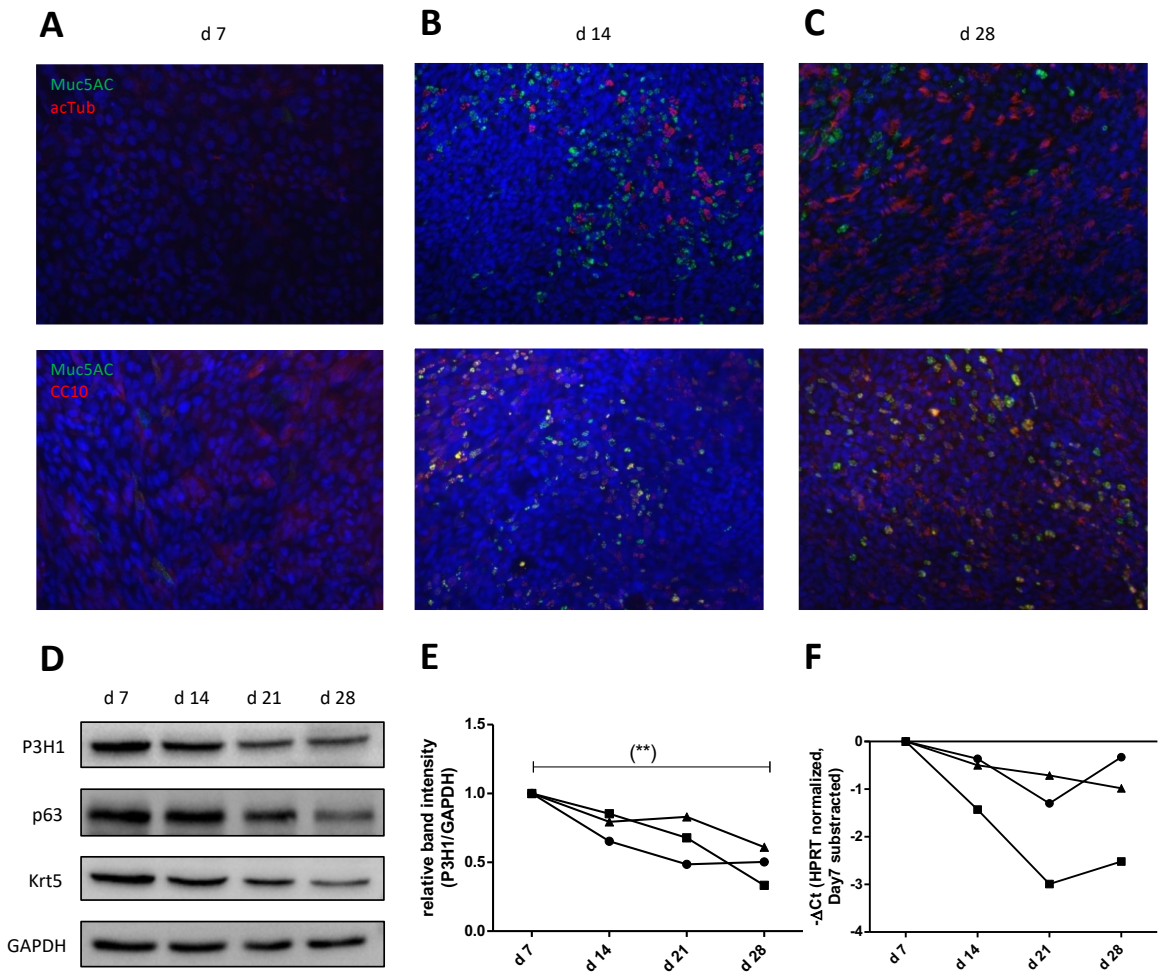

FIGURE 6: DIFFERENTIATION OF PHEBCS USING THE AIR-LIQUID-INTERFACE MODEL. (**A-C**) DIFFERENTIATING CELLS SHOWN AT DAY 7 (A), DAY 14 (B) AND DAY 28 (C) AFTER AIRLIFT. DAPI (BLUE), MUC5AC (GREEN) AND ACTUB (RED, FIRST ROW) / CC10 (RED, SECOND ROW). (**D**) REPRESENTATIVE WESTERN BLOT ANALYSIS OF P3H1, P63 AND KRT5 IN PHBEC LYSATES DURING 28-DAY DIFFERENTIATION. (**E**) GRAPHIC PRESENTATION OF P3H1 WESTERN BLOT ANALYSIS AS SHOWN IN (D), N = 3. (**F**) P3H1 TRANSCRIPT ANALYSIS BY QPCR, N = 3, DATA IS PRESENTED AS -ΔCT, NORMALIZED TO HPRT AND DAY 7. EACH LINE REPRESENTING ONE N. STATISTICAL ANALYSIS WAS PERFORMED USING ONE-WAY ANOVA. (**) INDICATING $P < 0.01$.

4.4 P3H1 IS REGULATED BY ER-STRESS INDUCERS, TGFß-1, AND MIR29B

4.4.1 ER-STRESS-INDUCING AGENTS TUNICAMYCIN AND THAPSIGARGIN PARTIALLY DOWNREGULATE P3H1 IN SUBMERGED PHBECS

The regulating mechanisms leading to differential P3H1 expression were assessed in undifferentiated pHBECs *in vitro*. Two ER-stress inducing agents, namely tunicamycin (TM) and thapsigargin (TG), were

applied to the submerged cells and cultured together with pure BEGM samples as controls. Binding immunoglobulin protein (BiP), also known as glucose-regulated protein 78 (GRP78), was used as validation for ER-stress in TM- and TG-treated samples. In cell lysates from TM-treated pHBECs, P3H1 analysis on western blot showed two differently sized fractions, a higher one correlating with the original protein size at 100 kDa, and a lower fraction at approximately 80 kDa (Figure 7, **A**). Comparing the total intensity of the scattered protein to the BEGM-control intensity, no significant difference was detected (Figure 7, **B**). TG led to significant decrease of P3H1 after 48 hours, with a concordant trend visible after 24 hours (Figure 7, **C**).

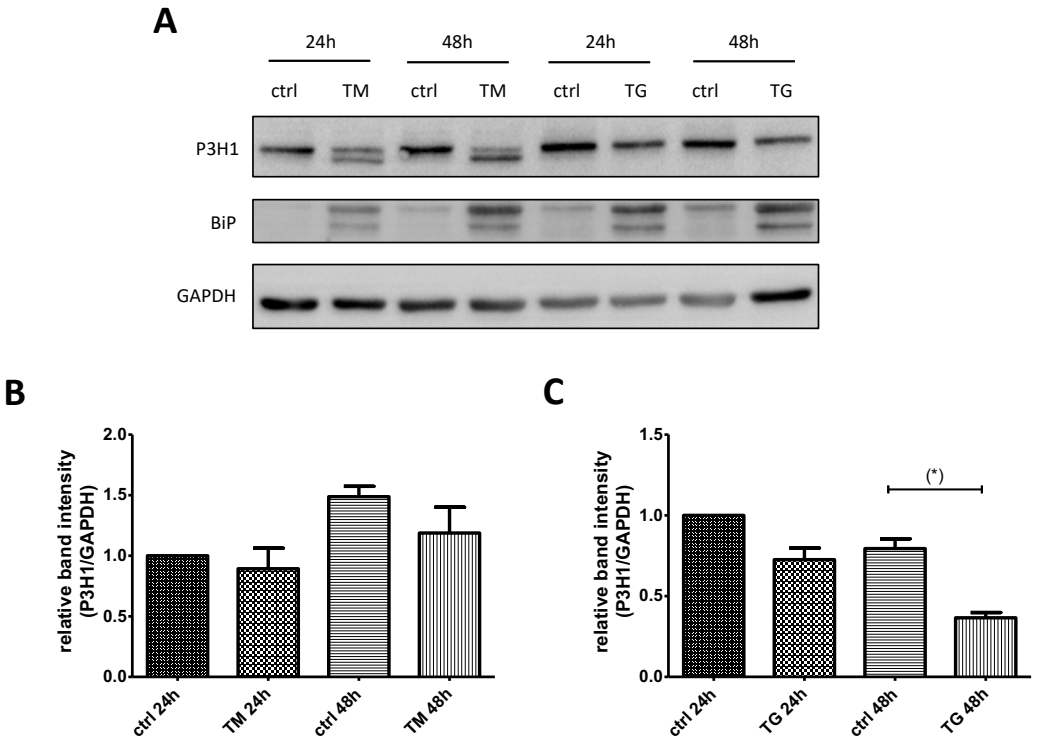

FIGURE 7: P3H1 PROTEIN DETECTION IN ER-STRESS-CHALLENGED PHBECS. (**A**) WESTERN BLOT ANALYSIS OF P3H1, ER-STRESS MARKER BIP AND HOUSEKEEPER GAPDH IN CONTROL (CTRL) AS WELL AS IN TUNICAMYCIN- (TM) AND THAPSIGARGIN- (TG) TREATED PHBEC LYSATES. (**B**) GRAPHIC PRESENTATION OF P3H1 WESTERN BLOT ANALYSIS IN TM-TREATED PHBECS, N = 3. (**C**) GRAPHIC PRESENTATION OF P3H1 WESTERN BLOT ANALYSIS IN TG-TREATED PHBECS, N = 3. MEAN ± SEM. STATISTICAL ANALYSIS WAS PERFORMED USING AN UN-PAIRED TWO-TAILED T-TEST. (*) INDICATING $P < 0.05$.

4.4.2 TGFß-1 INCREASES P3H1 PROTEIN AND TRANSCRIPT EXPRESSION IN PHBECS AFTER 24 HOURS

Submerged pHBECs were treated with 0 (pure BEGM control), 1 or 2 ng/ml TGFβ-1. In all replicates, rising phospho-SMAD3 levels and steady / decreasing total-SMAD3 indicated effective treatment.

P3H1 transcript analysis showed significant up-regulation with 2 ng/ml TGFβ-1 both after 24 hours and 48 hours (Figure 8, **C**). P3H1 protein levels were significantly increased after 24 hours, but the results remained inconclusive after 48 hours with almost no P3H1 expression difference with 1 ng/ml TGFβ-1 and non-significant decrease in pHBECs treated with 2 ng/ml TGFβ-1 (Figure 8, **A, B**).

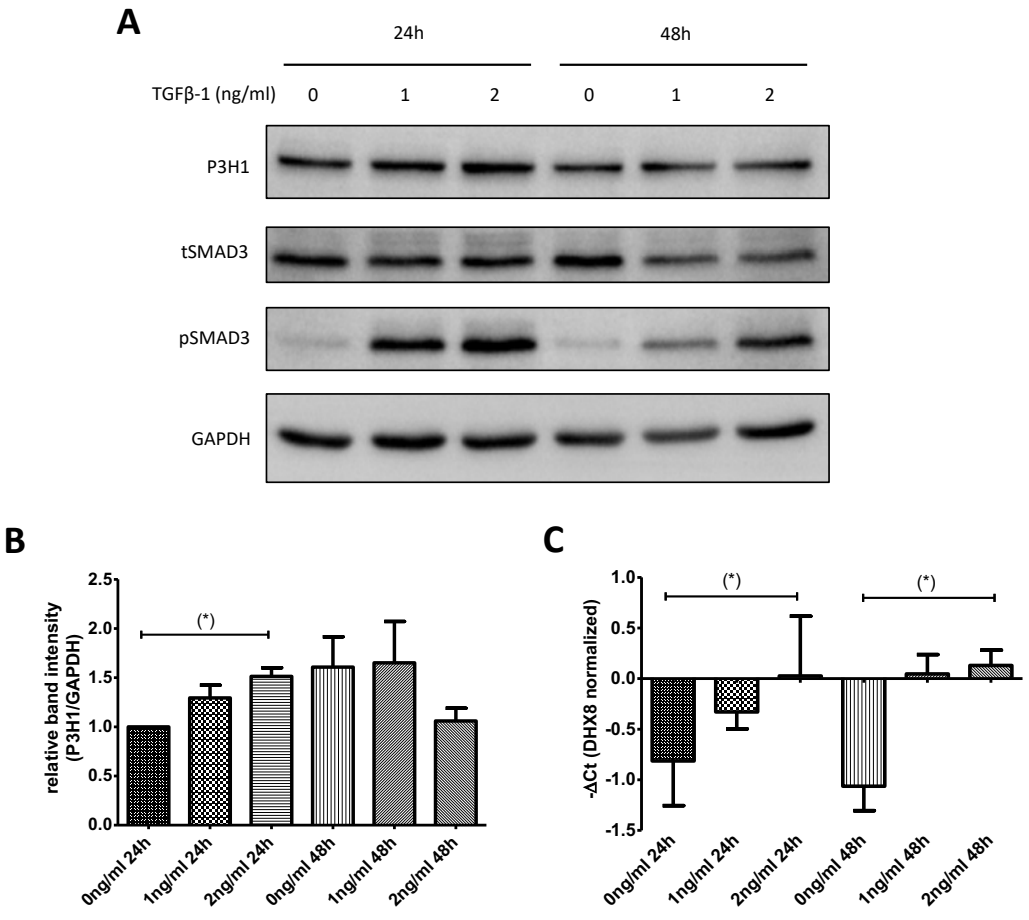

FIGURE 8: P3H1 PROTEIN AND TRANSCRIPT DETECTION IN TGFβ-TREATED PHBECS. (**A**) WESTERN BLOT ANALYSIS OF P3H1. (**B**) GRAPHIC PRESENTATION OF P3H1 RELATIVE BAND INTENSITY. N = 3. (**C**) P3H1 TRANSCRIPT ANALYSIS BY QPCR, DATA IS PRESENTED AS -ΔCT, NORMALIZED TO DHX8. N = 3. MEAN ± SEM. STATISTICAL ANALYSIS WAS PERFORMED USING AN UN-PAIRED TWO-TAILED T-TEST. (*) INDICATING $P < 0.05$.

4.4.3 pHBEC treatment with a miRNA29b inhibitor and precursor showed P3H1-regulation

The effect of microRNA29b on P3H1 expression was investigated by transfecting pHBECs with a miR29b inhibitor and precursor. Compared to control samples transfected with scrambled microRNA, inhibition of miR29b resulted in lower miR29b levels in pHBEC lysates, measured by Taq-Man based qRT-PCR, and precursor transfection successfully elevated miR29b levels (Figure 9, **A**).

SYBR green based qRT-PCR analysis of P3H1 mRNA 6 hours after transfection did not show significant effects with miR29b inhibitor or precursor treatment compared to controls. However, in pHBECs treated with the miR29b inhibitor for 24 hours, higher levels of the P3H1 transcript were detected and significantly lower levels with miR29b precursor treatment (Figure 9, **B**). P3H1 protein levels accordingly showed an increase upon miR29b inhibitor treatment and decrease with prescursor treatment both after 24 and 48 hours (Figure 9, **C, D**).

4.5 Evaluation of miR29b and collagen secretion in TGFß-1-stimulated pHBECs

P3H1 and miR29b transcript levels were assessed in TGFβ-1-treated pHBECs after 24 and 48 hours. The experiment was conducted in a different cell line than the previously shown TGFβ-1 regulation assays. Firstly, dose-dependent P3H1 transcript up-regulation with 1 and 2 ng/ml TGFβ was confirmed (Figure 10, **A**). Secondly, Taq-Man based qRT-PCR did not show significant miR29b expression changes with neither 1 nor 2 ng/ml TGFβ-1 (Figure 10, **B**).

Cell culture supernatants were harvested after 24 and 48 hours and collagen deposition was assessed using the Sircol Assay. Compared to controls, treatment with both 1 and 2 ng/ml TGFβ-1 resulted in mildly elevated collagen secretion after 24 and 48 hours. The observed effect was overall not dose-dependent (Figure 10, **C**).

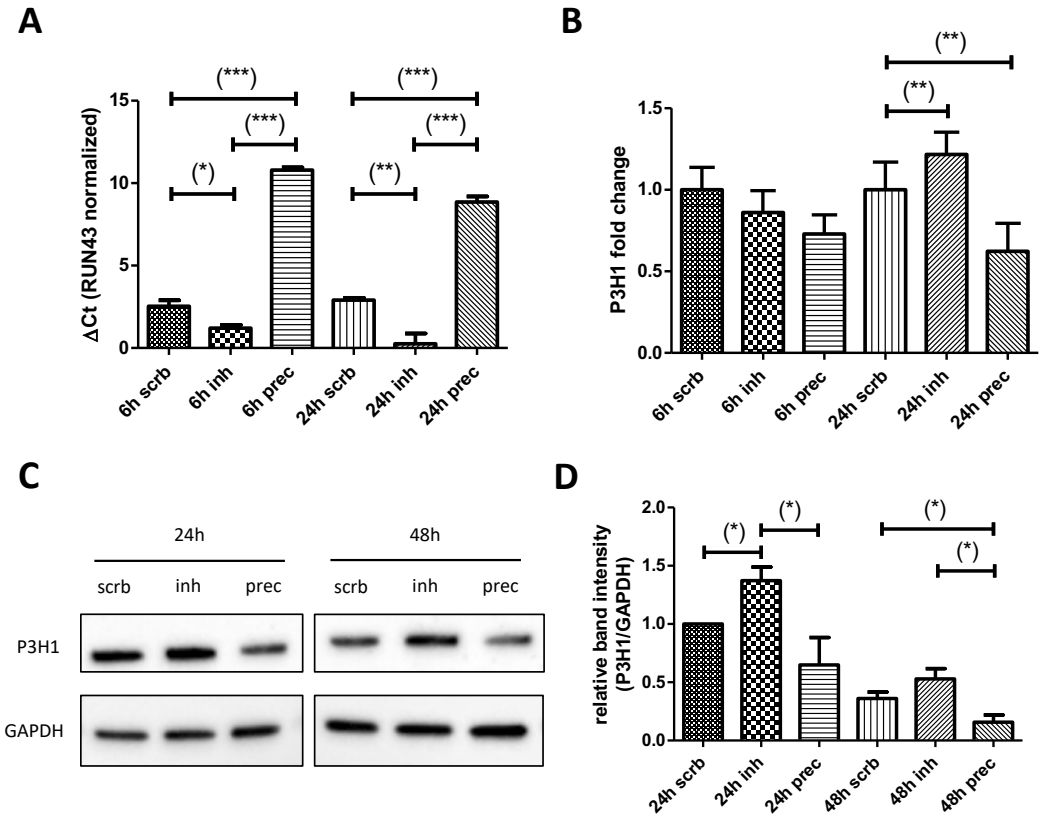

FIGURE 9: REGULATION OF P3H1 PROTEIN AND MRNA BY MIR29B INHIBITOR AND PRECURSOR. (**A**) MIR29B TRANSCRIPT ANALYSIS BY QPCR IN PHBEC LYSATES TREATED WITH SCRAMBLED CONTROL (SCRB), MIR29B INHIBITOR (INH) AND MIR29B PRECURSOR (PREC). DATA POOLED FROM FOUR QPCR ANALYSIS REPLICATES FROM ONE BIOLOGICAL EXPERIMENT. DATA IS PRESENTED AS ΔCT, NORMALIZED TO RNU43. (**B**) FOLD CHANGES OF P3H1 MRNA ANALYZED BY QPCR. (**C**) WESTERN BLOT ANALYSIS OF P3H1 IN MIR29B-TREATED PHBECS. (**D**) GRAPHIC PRESENTATION OF FOUR ANALYSIS REPLICATES FROM ONE BIOLOGICAL EXPERIMENT. MEAN $\pm$ SEM. STATISTICAL ANALYSIS WAS PERFORMED USING AN UN-PAIRED TWO-TAILED T-TEST. (*) INDICATING $P < 0.05$, (**) $P < 0.01$, (***) $P < 0.001$.

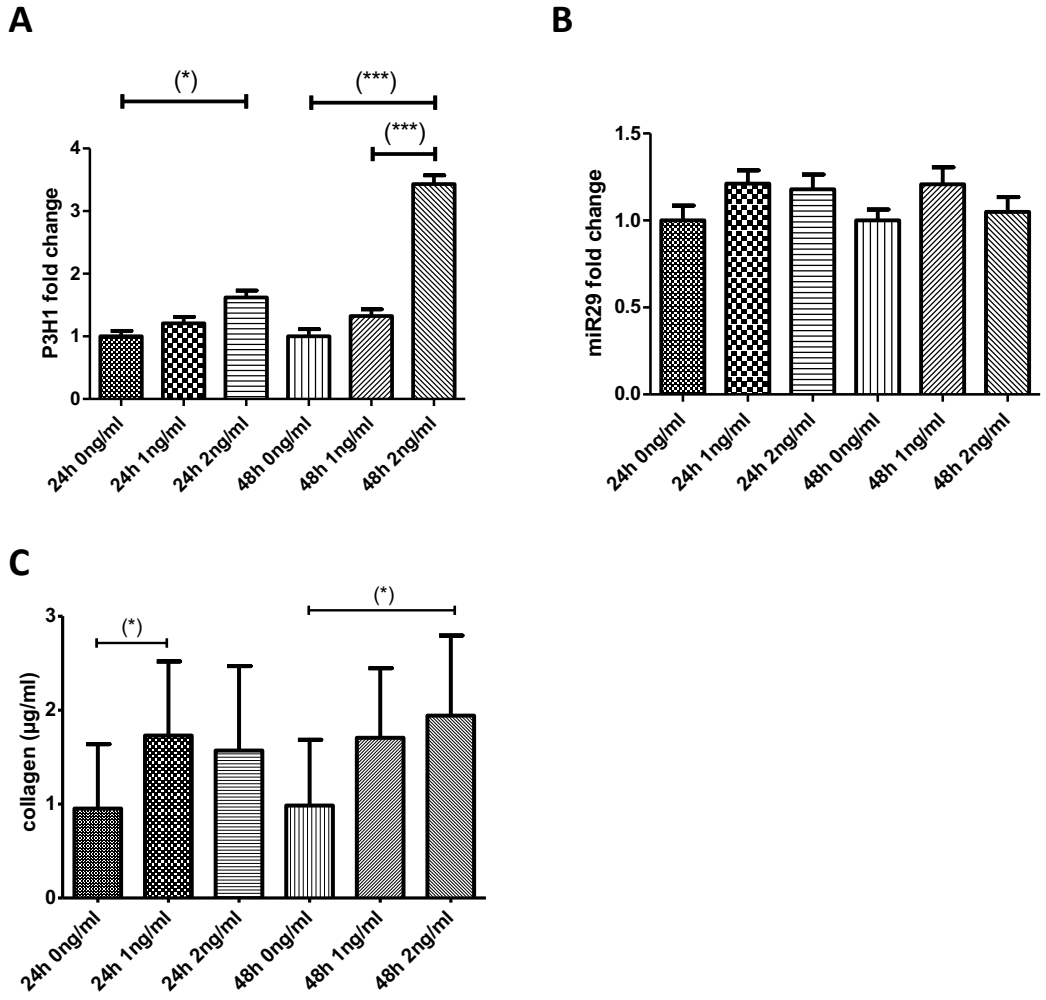

FIGURE 10: P3H1 AND MIR29B TRANSCRIPT AND COLLAGEN DETECTION IN TGFβ-TREATED PHBECS. (**A, B**) FOLD CHANGES OF P3H1 MRNA (A) AND MIR29B (B) IN PHBEC LYSATES. FOUR QPCR REPLICATES POOLED FROM ONE BIOLOGICAL EXPERIMENT. (**C**) SECRETED COLLAGEN IN TGFβ-TREATED PHBEC SUPERNATANTS MEASURED BY SIRCOL ASSAY. N = 3. MEAN ± SEM. STATISTICAL ANALYSIS WAS PERFORMED USING AN UN-PAIRED TWO-TAILED T-TEST. (*) INDICATING $P < 0.05$. (***) $P < 0.001$.

4.6 P3H1 SILENCING EXPERIMENTS IN PHBECS

4.6.1 REVERSE KNOCKDOWN IN DIFFERENTIATING BRONCHIAL EPITHELIAL CELLS SHOWS SILENCING OF P3H1 ON PROTEIN AND TRANSCRIPT LEVEL FOR 192 HOURS

In preparation of the functional analysis of P3H1 in differentiating pHBECs, a pilot knockdown experiment was conducted by reverse transfection of pHBECs on transwell membranes with P3H1

siRNA (10 nM). The cells were airlifted 48 hours after the transfection, protein and RNA samples were obtained 48, 72, 144 and 192 hours after the transfection.

P3H1 mRNA levels were decreased in siRNA-transfected cells at all observed time points, suggesting stable silencing of P3H1 for 192 hours in this *in vitro* model (Figure 11, **B**). On protein level, P3H1 expression was substantially decreased in knockdown samples (Figure 11, **A**). To clarify the effect of P3H1 knockdown on the pHBEC differentiation process in the Air-Liquid-Interface model, a serial transfection approach was tested to achieve stable P3H1 silencing for four weeks. Therefore, two transwells were initially airlifted and cultured with pure ALI-medium for 192 hours and then transfected with scrambled or P3H1 siRNA for 48 hours. No depletion of the P3H1 transcript resulted from this experiment (Figure 11, **C**).

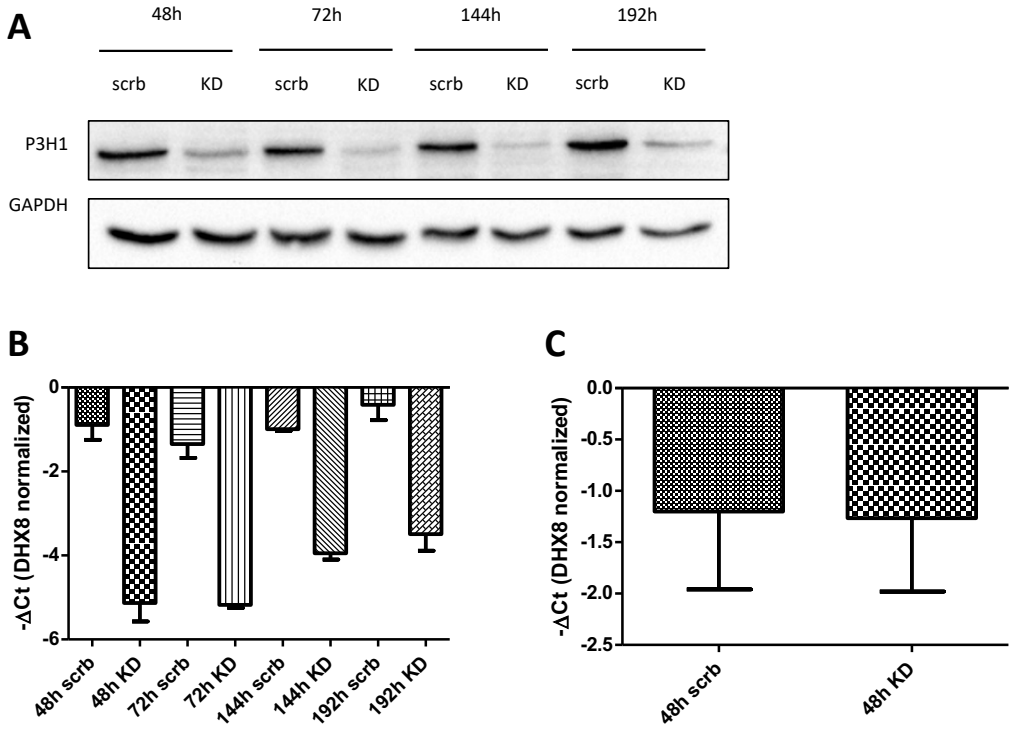

FIGURE 11: P3H1 KNOCKDOWN IN DIFFERENTIATING PHBECS. (**A**) WESTERN BLOT ANALYSIS OF SCRAMBLED CONTROL (SCRB) AND P3H1 SIRNA TRANSFECTED (KD) DIFFERENTIATING PHBECS. (**B, C**) P3H1 TRANSCRIPT ANALYSIS BY QPCR IN DIFFERENTIATING TRANSFECTED PHBECS AT 0 HOURS (B) AND 192 HOURS (C). DATA IS PRESENTED AS -ΔCT, NORMALIZED TO DHX8. N = 2. MEAN ± SEM.

4.6.2 Reverse transfection with P3H1 siRNA in submerged pHBECs succeeded in P3H1-silencing for 72 hours

In submerged pHBECs (10,000 cells /cm^2), reverse transfection with 10 nM P3H1 siRNA resulted in protein and mRNA knockdown after 48 and 72 hours (Figure 12, **A, B**). Forward transfection (10,000 cells /cm^2) did not succeed in silencing P3H1 on protein level after 48 hours, but after 72 hours, whereas the P3H1 transcript was downregulated at both time points (Figure 12, **D, E**). In addition, the reverse knockdown experiment was performed with doubled initial pHBEC count. Accordingly, effective P3H1 protein depletion was achieved in 20,000 cells /cm^2 on protein level after 72 hours (Figure 12, **C**).

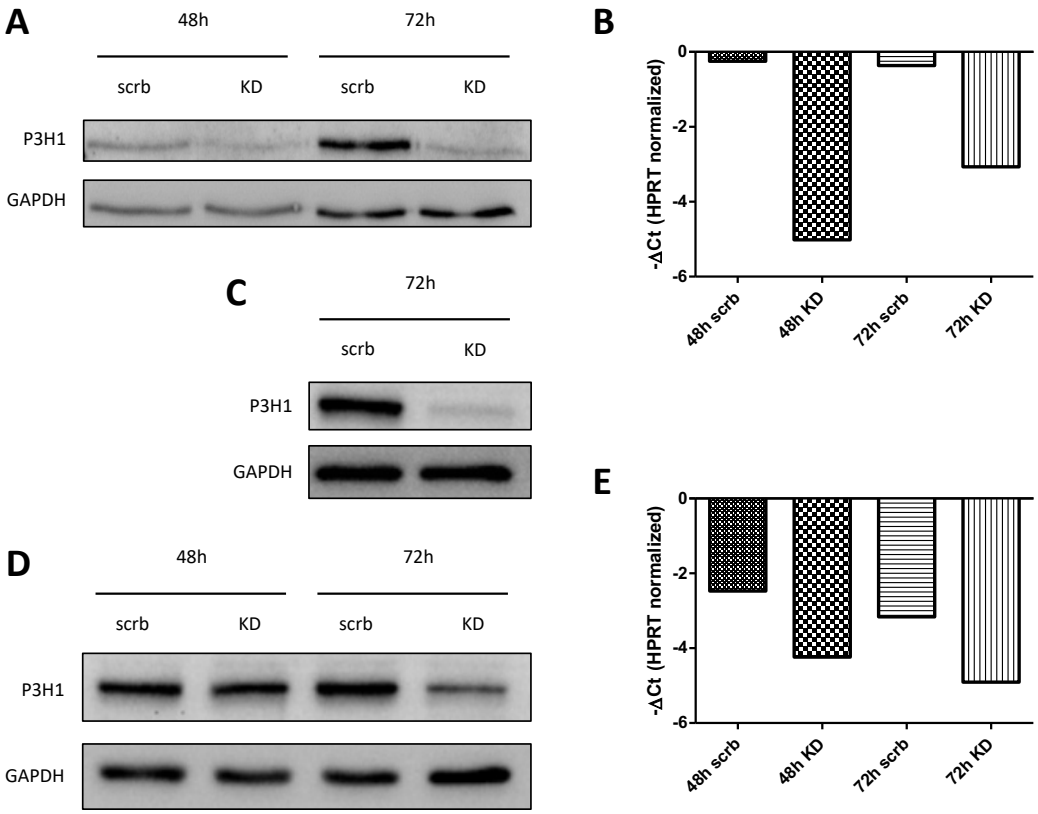

FIGURE 12: P3H1 KNOCKDOWN IN SUBMERGED PHBECS. (**A, B**) WESTERN BLOT (A) AND QPCR (B) ANALYSIS OF SCRAMBLED CONTROL (SCRB) AND P3H1 SIRNA TRANSFECTED (KD) SUMBERGED PHBECS USING REVERSE TRANSFECTION AND 10,000 CELLS /CM^2. TRANSCRIPT DATA PRESENTED AS -ΔCT, NORMALIZED TO HPRT. N = 1. (**C**) WESTERN BLOT ANALYSIS USING REVERSE TRANSFECTION AND 20,000 CELLS /CM^2. (**D, E**) WESTERN BLOT (D) AND QPCR (E) ANALYSIS USING FORWARD TRANSFECTION AND 10,000 CELLS /CM^2. TRANSCRIPT DATA PRESENTED AS -ΔCT, NORMALIZED TO HPRT. N = 1.

4.7 FUNCTIONAL ASSAYS DISPLAY THE INFLUENCE OF P3H1 ON BASAL CELL MARKER EXPRESSION AND PHBEC PROLIFERATION *IN VITRO*

4.7.1 P63 IS UPREGULATED UPON P3H1-KNOCKDOWN IN PHBECS

In submerged pHBECs, P3H1 knockdown was performed for 72 hours and additionally 2 ng/ml TGFβ-1 and control treatment 24 hours after transfection (Figure 13, **A**). In protein lysates, p63 was upregulated in P3H1 depleted samples (Figure 13, **C**). TGFβ-1 did not have significant effects on p63 expression, but elevated P3H1 in scrambled controls by an approximate 1.5-fold resembling previous results (Figure 13, **B**).

In differentiating pHBECs, airlifted and transfected at 0 hours, p63 transcript expression was measured using qRT-PCR at 48, 72, 144 and 192 hours (Figure 13, **D**). Notably, remarkable changes in expression of the endogenous control DHX8 were observed, which may have influenced -ΔCt calculations. Elevated p63-levels in P3H1 knockdown condition for the early differentiation period may therefore not be fully reliable.

4.7.2 P3H1 KNOCKDOWN DECREASES PROLIFERATION OF SUBMERGED PHBECS IN PRESENCE OF TGFβ-1, BUT DOES NOT AFFECT PCNA LEVELS

pHBEC proliferation in P3H1 knockdown and TGFβ-1 condition was assessed using the BrdU assay. The cells were seeded in three densities (40,000, 80,000 and 160,000 pHBECs /cm^2) and simultaneously transfected with P3H1 siRNA / scrambled control, treated with 2 ng/ml TGFβ-1 after 24 hours following BrdU uptake evaluation after another 48 hours.

TGFβ-1 significantly decreased BrdU uptake in all conditions compared to controls without TGFβ-1-stimulation. More importantly, there was also a significant decrease in BrdU uptake in P3H1-depleted pHBECs compared to the scrambled controls in presence of TGFβ-1, which is similar in every cell density (Figure 14, **A**). The effect was also visible in the two non-TGFβ-1 groups with low and medium cell density (40,000 and 80,000 cells per cm^2).

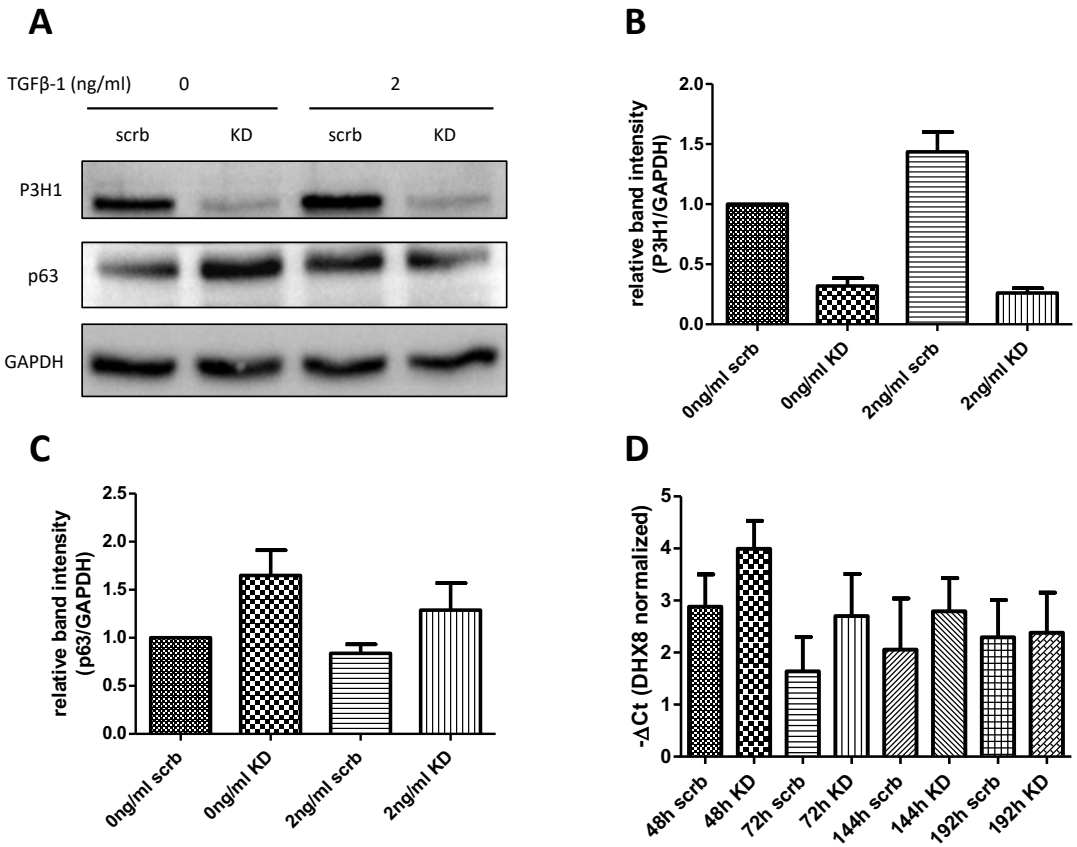

FIGURE 13: EVALUATION OF P63 IN P3H1-DEPLETED AND TGFβ-TREATED PHBECS. (**A**) REPRESENTATIVE WESTERN BLOT OF SUBMERGED, P3H1-SIRNA-TRANSFECTED PHBECS IN CONTROL AND TGFβ ENVORINMENT. SCRAMBLED CONTROL (SCRB) AND P3H1 KNOCKDOWN (KD). N = 3. (**B, C**) GRAPHIC PRESENTATION OF P3H1 (B) AND P63 (C) RELATIVE BAND INTENSITY AS SHOWN IN (A). N = 3. (**D**) P63 TRANSCRIPT ANALYSIS USING QPCR IN LYSATES OF DIFFERENTIATING PHBECS. 0H REPRESENTS TIME OF AIRLIFT. DATA PRESENTED AS -ΔCT, NORMALIZED TO DHX8. N = 2. MEAN ± SEM. STATISTICAL ANALYSIS WAS PERFORMED USING AN UN-PAIRED TWO-TAILED T-TEST. SIGNIFICANCE WAS ONLY DETECTED FOR 0 NG/ML TGFβ SCRB VS. KD AND 2 NG/ML TGFβ SCRB VS. KD, RESPECTIVELY (NOT SHOWN).

In submerged pHBECs, the Proliferating Cell Nuclear Antigen (PCNA) was evaluated to determine the influence of P3H1 knockdown on pHBEC proliferation in a second approach. Therefore, P3H1 reverse knockdown with subsequent TGFβ-1 treatment was conducted. Compared to scrambled controls, no significant differences in PCNA levels could be detected in P3H1 knockdown samples on western blot (Figure 14, **B, C**).

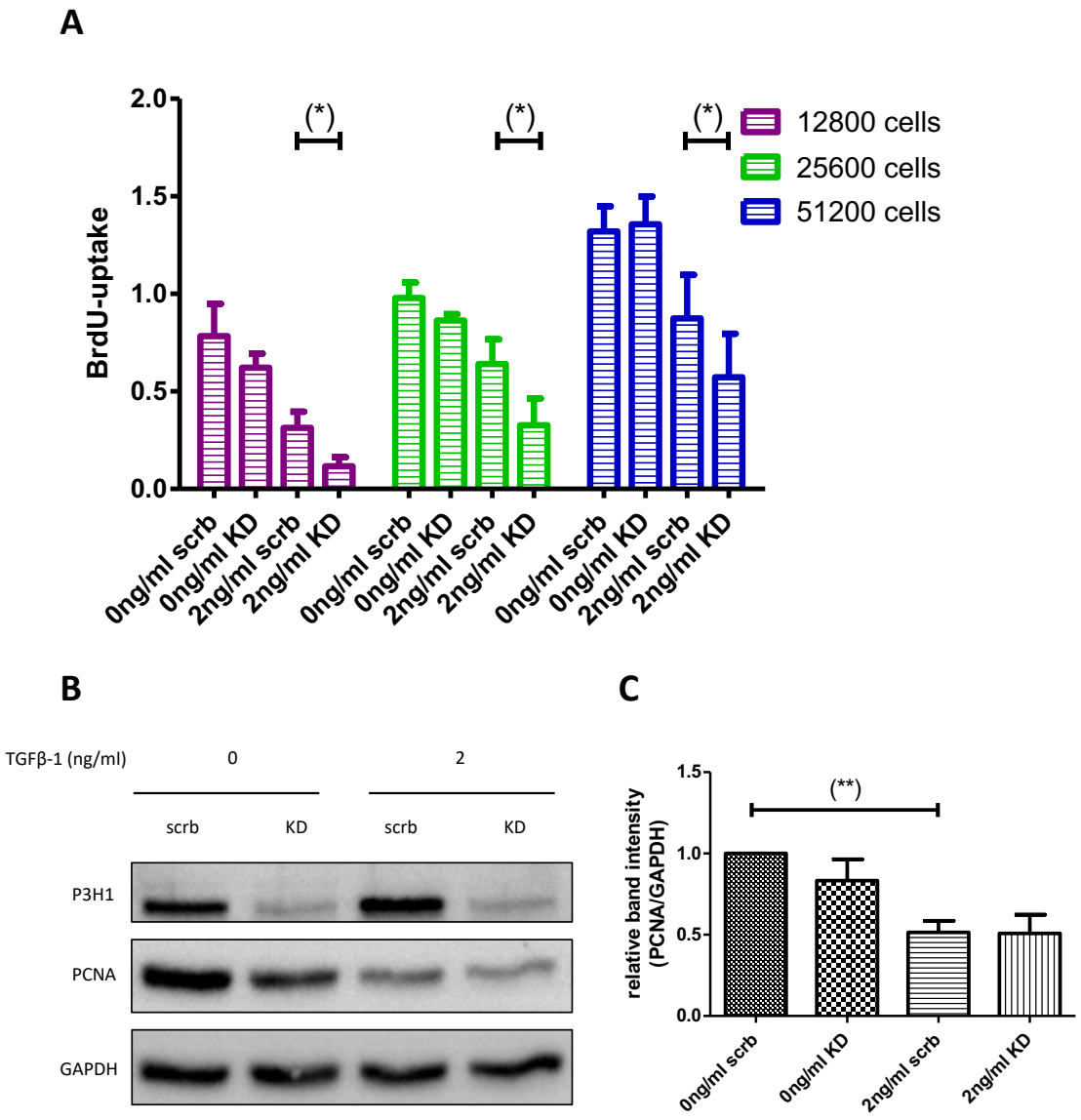

FIGURE 14: PROLIFERATION IN P3H1-DEPLETED PHBECS. (**A**) BRDU UPTAKE IN SUBMERGED PHBECS TREATED WITH SCRAMBLED CONTROL (SCRB) AND P3H1 SIRNA (KD) AS WELL AS TGFβ-1 (2 NG/ML) AND CONTROL (0 NG/ML). THE EXPERIMENT WAS CONDUCTED IN THREE CELL DENSITIES (40,000 [PURPLE], 80,000 [GREEN] AND 160,000 [BLUE] PHBECS /CM²). N = 3. BRDU UPTAKE WAS SIGNIFICANTLY LOWER IN ALL TGFβ-1-TREATED SAMPLES COMPARED TO THE CORRESPONDING CONTROL (NOT SHOWN) (**B**) REPRESENTATIVE WESTERN BLOT ANALYSIS OF P3H1 AND PCNA IN P3H1 KNOCKDOWN AND TGFβ-TREATED PHBECS. (**C**) GRAPHIC PRESENTATION OF RELATIVE PCNA BAND INTENSITY AS SHOWN IN (B). N = 3. MEAN ± SEM. STATISTICAL ANALYSIS WAS PERFORMED USING AN UN-PAIRED TWO-TAILED T-TEST. (*) INDICATING $P < 0.05$, (**) $P < 0.01$.

5 DISCUSSION

5.1 EXPRESSION AND DISTRIBUTION OF P3H1 IN IPF

The bleomycin mouse model is widely being used as the standard murine model for interstitial lung fibrosis in preclinical research, leading the way for the ongoing unveiling of IPF pathogenesis and clinical trials.[46,47] However, the model features important differences to human IPF, e.g. spontaneous retrogression of fibrosis only 3-4 weeks after bleomycin administration.[48] Insights from murine experiments therefore need to be applied to human specimen to further characterize differences between animal and human fibrogenesis and to continue the search for key pathogenetic proteins that could potentially serve as drug targets.

The data presented here follows up on a comprehensive proteomics dataset published by Schiller et al. on protein expression in bleomycin-induced pulmonary fibrosis (BIPF) in mice.[43] Three proteins involved in collagen prolyl-hydroxylasis, namely P3H1, P3H2 and CRTAP, were found to be elevated in BIPF. In IPF lung tissue homogenates from the CPC-M biobank and the LTRC biobank, P3H1 was increased compared to histologically disease-free human lung tissue. Despite considerable variability within the two groups, the overall increase was significant. The genetic component of IPF as well as its clinical presentation at diagnosis and response to treatment are known to be heterogenous, which may explain the observed variability in between IPF samples, which have not been characterized in regard to individual disease severity.[8,49–51] Subsequently, IF-stainings for P3H1 in IPF confirmed increased P3H1 levels compared to HC tissue. P3H2 and CRTAP did not show differential expression for the expected protein size on western blot analysis, even though a 70 kDa variant of P3H2 was elevated in IPF samples. Whether this variant is a P3H2 isoform or a deglycosylated version of the canonical sequence remains inconclusive.

mRNA expression analysis in six samples from the CPC-M biobank did not show expression differences between HC and IPF in P3H1 and CRTAP, whereas the P3H2 transcript was significantly lower in IPF samples. Equivalent results have been published in a transcriptomics dataset by Kaminski et al. in 2005.[52–54] Conclusively, only CRTAP out of the three analyzed proteins may be directly regulated by mRNA quantity, but for P3H1 and P3H2, posttranscriptional regulation mechanisms seem to be in play.[55]

The histopathologic classification of IPF tissue has been implicated as part of the diagnostic work-up in inconclusive cases of interstitial lung disease.[6] Current guidelines describe the usual interstitial

pneumonia (UIP) pattern – the most common histopathologic pattern in IPF patients – as marked architectural distortion of lung parenchyma with or without subpleural / paraseptal cysts or honeycombing, patchy fibrosis featuring fibroblast foci and absence of features against UIP-diagnosis.[6] Over the last years, many publications elaborated the activation of (myo)fibroblasts and their role of driving fibrosis through collagen production and modification.[56,57] Interestingly, αSMA-positive myofibroblasts did not predominantly express P3H1 *in situ*, as is the case for other collagen-modifying enzymes.[44] The initial insight of P3H1 staining around small airways led to a series of IF-stainings, in which P3H1 co-located with basal cell markers p63 and Krt14 in IPF. In pHBEC lysates, P3H1 mimicked the basal cell marker p63 and Krt5 concentration drop over the 28-day differentiation period, suggesting pHBECs to be the major P3H1 expressing cell type in a different experimental approach. While human airway basal cells from healthy individuals were known to produce various types of collagens (e.g. COL4A1, COL17A1) and Integrin alpha 6, as well as P3H2, suggesting, that the cells are involved in ECM production, but also facilitate cell-matrix interactions and migration,[58,59] only recently, bronchoalveolar lavage (BAL) from IPF patients showed enrichment in airway basal cells and their transcriptome profile was predictive for mortality.[60]

Senescent bronchoalveolar epithelium is hypothesized to result from the various personal, genetic and environmental risk factors for the development of IPF, e.g. age, smoking history, Muc5B promoter variants, dust inhalation, micro-aspiration and recurrent infections.[61–63] Much like a gatekeeper of consecutive lung remodeling, the damaged epithelium then activates myofibroblasts and immune cells, leading to abnormal – referring to both quality and quantity – ECM-deposition.[61,64,65] Some studies also show evidence of airway and alveolar epithelial cells acquiring a mesenchymal expression signature, suggesting a phenomenon called epithelial to mesenchymal transition (EMT) to contribute to fibrogenesis.[66,67] Besides ECM deposition, a striking structural change is the development of (honeycomb) cysts and although recent data from CT scans on explant lungs revealed the branching structure of the cysts on a macroscopic level,[68] the histopathologic characteristics of the epithelial lining and its possible involvement in fibrogenesis remain unclear. The IF-images presented here remarkably show two types of epithelium, one of which appears to be similar in marker expression to the contrasted healthy control bronchial epithelium featuring ciliated, goblet and clara cells as well as few $p63^+$ basal cells, whereas the other type apparently lacks specialized cells while the remaining basal cells exhibit an altered expression profile ($p63^+$ / $Krt14^+$ / $P3H1^+$). In fact, the latter could represent the epithelium of a (honeycomb) cyst with loss of normal airway function, similar to what has been observed by Jonsdottir and others.[66,69] Considering the apparent switch in basal cell expression profile and absence of specialized epithelium, these images may insinuate a link between P3H1 expression and abnormal development of airway epithelium.

5.2 REGULATION OF P3H1 IN PHBECS

To characterize the regulation of P3H1 *in vitro*, pHBECs have been analyzed regarding P3H1 mRNA and protein expression after treatment with known stimuli of lung fibrogenesis.

Endoplasmic reticulum (ER) stress in general refers to a state of incapability of regular protein folding and quality control, which leads to accumulation of misfolded and dysfunctional proteins within the ER, activation of salvage mechanisms and ultimately apoptosis.[70,71] In the context of IPF, ER-stress can be caused by genetic mutations in the surfactant protein A2 gene, cellular ageing, micro-particle inhalation, mechanical stress and hypoxia.[72–76] Depending on the predominantly affected cell type, various profibrotic mechanisms are launched including activation of myofibroblasts and inflammatory signaling.[77–79] Both tunicamycin and thapsigargin evoke cellular response mechanisms to ER-stress *in vitro*, and both agents affected P3H1 expression in pHBECs. Tunicamycin, which functions as a glycosylation inhibitor scattered the original western blot band into two fractions, one of which is likely to represent the original protein at 100 kDa, whereas the lower fraction may resemble a de-glycosylated protein variant at approximately 85 kDa, which in fact matches the predicted protein size without posttranslational modifications.[33] Thapsigargin, a sarcoplasmic / endoplasmic reticulum calcium ATPase inhibitor, on the other hand, decreased P3H1 concentrations without affecting its size. This finding contradicts the hypothesis, that ER-stress is solely responsible for the expression profile of the observed $P3H1^{+}$ basal cell population in IPF, however, further investigation is needed to clearly determine, if ER-stress is present in the aberrant bronchial epithelium and if it correlates with P3H1 / Krt14 expression *in situ*. Besides, the unfolded protein response (UPR), one of the cell's reactions to cope with ER-stress and regain protein homeostasis, temporarily increases chaperone and redox enzyme expression, but decreases general translation of proteins dispensable for survival, as has been shown for the collagen chaperone FKBP10.[44,80] This mechanism might also be an explanation for the observed P3H1 downregulation.

TGFß is one of the pivotal profibrotic cytokines and its role in IPF has been investigated in great detail.[24] Facing persistent injury, the damaged epithelium is known to induce fibrotic changes in the interstitium through a cocktail of fibrogenic cytokines including TGFß, PDGF, IL-10 and Wnt / WISP1, but conversely, TGFß secreted from activated myofibroblasts also reinforces epithelial cell death.[24,81–85] This vicious cycle has mainly been characterized in alveolar epithelial cells, but given the proximity of airways and myofibroblast foci, the paracrine influence on bronchial epithelial cells is putative. The data presented here shows in a number of different experiments, that P3H1 is elevated

through TGFß-1 in pHBECs by roughly 1.5-fold, providing a plausible mechanism for its overexpression in IPF.

Total collagen secretion roughly doubles in fibroblasts derived from IPF lungs after 48 hours of TGFß-1 treatment *in vitro*.[44] Using the same collagen detection technique, collagen secretion from healthy pHBECs also showed an increase with TGFß-1 treatment, but in both treated and control samples, the amount of secreted collagen was close to the lower detection limit of the performed sircol assay at 1 µg/ml.[86] This result suggests, that bronchial epithelial cells from disease free human lungs are not capable of producing relevant quantities of collagen to step out of the shadow of (myo)fibroblasts as the main effector cells of hyperplastic ECM-deposition. Inborn or acquired genetic variations or expression switches may, however, lead to less subtle changes in quantity of secreted collagen by TGFß-1 in airway basal cells.

Among the inexhaustible factors and pathways shaping IPF into the complex disorder it is known for, microRNA29 – a small non-coding RNA molecule suppressing multiple ECM-related genes – has been established as yet another key factor.[87,88] Since the absence of miR29 is proven to drive fibrosis, replacement therapies pose as an elegant new approach to tackle IPF. After successful advances of treating bleomycin-induced fibrosis with intravenous recombinant miR29 in mice, inhaled treatment options are now on the verge of being evaluated in clinical trials.[46] Many profibrotic cytokines, specifically TGFß, were reported to downregulate miR29 in HK2 cells,[89] fetal lung fibroblasts,[90] hepatic stellate cells,[91] and kidney fibroblasts,[92] which results in an aberrant would healing process and potentiated matrix deposition. Whereas no suppression of miR29b by TGFß-1 was evident in pHBECs, two independent databases for microRNA targets predicted miR29b to bind the P3H1-3'UTR.[93,94] Even though the P3H1 transcript does not seem to be affected 6 hours after transfection, P3H1 protein expression increased in absence of miR29b and equally decreased in miR29b-precursor transfected cells, which after 24 hours matches mRNA expression. This result allows just another glimpse at a possible mechanism of P3H1 regulation, given the experiment was only conducted in one biological replicate and the interaction of microRNA29b and other modulators *in vivo* remains to be investigated.

5.3 FUNCTIONAL ANALYSIS OF P3H1 IN BRONCHIAL EPITHELIAL CELLS

In a preparatory step towards analyzing the function of P3H1 in pHBECs *in vitro*, pilot knockdown experiments showed stable P3H1 suppression in submerged and differentiating cells on the air-

liquid-interface for 72 and 192 hours, respectively. Airlifted cells were also transfected at 192 hours to evaluate serial transfection as a method of P3H1 silencing over the 28-day differentiation timeline, which did not prove efficient. Transfection with short hairpin RNA or the use of lentiviral vectors may be qualified alternatives.[95]

p63 transcript expression was upregulated in P3H1 depleted differentiating pHBECs. The validity of this result is debatable considering the lack of stability of the housekeeper gene DHX8. Submerged pHBECs treated with P3H1 siRNA, however, also showed p63 increase on protein level.

p63 together with p53 and p73 comprises a family of tumor suppressor proteins, and has only been identified and characterized in the last 25 years.[96,97] The p63 DNA-binding domain matches the corresponding p53 domain sequence by more than 60%, but N- and C-terminal appendages vary and determine the functional capabilities of p63 isotypes.[97] Whereas one subgroup, which is expressed in ovarian cells and equipped with an amino-terminal transactivation domain (TA-p63), mimics the functional characteristics of p53, ΔN-p63 isotypes, which occur in epithelial tissues, antagonize p53 by maintaining regenerative capacities of epithelial stem cells.[97–100] $p63^{-/-}$ mice accordingly feature dysfunctional stratified epithelial tissues and truncated limbs,[101–103] and p63 knockdown in primary human airway epithelial cells decreased various genes associated with epithelial repair and differentiation.[104]

The experiments in pHBECs, the surrogate of the lung's basal cell population, suggest an increase of p63, the key protein to well-functioning epithelial differentiation and repair, in absence of P3H1. The data presented here also shows increased P3H1 levels in basal cells of IPF lungs, which may in turn lead to degradation or deactivation of p63 and consequently an imbalanced state of proliferation and differentiation of these central airway progenitors.

Even though p63 is not known to be a direct target of P3H1, interactions with cell proliferation and differentiation have been discovered for various prolyl-hydroxylases. Prolyl-4-hydroxylase α-1 (P4HA1) is expressed in triple-negative and HER2-positive breast cancer tissue, where it protects hypoxia-inducible factor 1α (HIF-1α) from proteasome degradation by reducing egl nine homolog 1 (PHD2) -mediated proline hydroxylation.[105] High levels of HIF-1α facilitate cancer progression, but it also physiologically reduces proliferation in multiple cell lines as a reaction to hypoxia.[106] Another study found suppression of cell proliferation by ectopic expression of P3H2 and P3H3.[107,108] Growth suppressor 1L (GROS1L) is identical with a cytoplasmatic form of P3H1 and suppresses proliferation in NIH3T3 cells, a murine fibroblast cell line.[109]

In IF-staining of IPF lung tissue, airways featuring P3H1^{-} / Krt14^{-} / p63^{+} basal cells and expression of differentiation markers mimicked airways from healthy controls, but P3H1 was present in a distinct population of Krt14^{+} / p63^{+} basal cells. The striking absence of ciliated, goblet and clara cells above these denuded P3H1^{+} progenitors may indicate a correlation between P3H1 expression and lacking capability to fully differentiate into bronchial epithelium. Distal airways of IPF lungs are known to host a dominant subpopulation of Krt5^{+} / Krt14^{+} basal cells.[110] In this study, bronchial epithelial differentiation markers were also not detected in areas featuring this particular subpopulation.[110]

pHBEC proliferation, assessed by BrdU uptake measurement, was decreased in TGFβ-1 treated cells, but also in P3H1-depleted cells in a TGFβ-1 environment. This finding was initially not supported by a separate analysis of the proliferation marker PCNA, which was not altered by P3H1 knockdown but only in TGFβ-1-treated and scrambled control transfected cells. Notably, all experiments presented here were conducted without synchronization of pHBECs' cell cycles prior to transfection with P3H1 siRNA and TGFβ-1 treatment. In an attempt to clarify the validity of the BrdU assay and its findings, PCNA evaluation was repeated by Elisabeth Hennen at a later stage including synchronization of pHBECs using starvation media (unpublished data, with permission of Staab-Weijnitz Lab). These experiments were able to demonstrate PCNA decrease in a P3H1 knockdown condition in agreement with the BrdU assay results. TGFβ inhibits proliferation in a variety of epithelial cell types, such as alveolar epithelial type II cells.[82,111] The observed correlation between P3H1 knockdown and decreased pHBEC proliferation, however, has not been described to date.

Certainly, this data only provides limited evidence of a causal mechanism linking P3H1 to the complex epithelial differentiation and regeneration process. Co-immunoprecipitation may be able to clarify, if there is a direct interaction of P3H1 with p63, even though IF-stainings in IPF located the two proteins in separate cellular compartments. Further analysis of the core function of P3H1 may elaborate, if IPF airway progenitors produce a differently modified basement membrane, which invokes cellular responses not only in bronchial epithelial cells, but also in resident fibroblasts. Parker and colleagues demonstrated, that the composition of ECM has greater impact on fibroblast transcriptome and translatome, than their actual origin from fibrotic or healthy lungs.[56] Knockdown and knock-in of P3H1 during the four-week differentiation of pHBECs may finally provide a more profound insight, if P3H1 expression leads to altered -omics and epithelial differentiation.

6 CONCLUSION

In this study, P3H1 was found to be elevated in total lung lysates of IPF patients from two independent cohorts and located in $Krt14^+$ / $p63^+$ airway basal cells. The $P3H1^+$ / $Krt14^+$ / $p63^+$ cell population was present in airways exclusive of differentiated bronchial epithelial cells. *In vitro* experiments with pHBECs indicated the influence of two key fibrotic regulators TGFβ and miR29b on P3H1 transcript and protein expression. P3H1 knockdown in pHBECs resulted in elevation of the epithelial differentiation modulator p63 as well as in decrease of proliferative activity. Taken together, the data suggests P3H1 to be involved in the formation of an aberrant bronchial epithelium, possibly even in development of (honeycomb) cysts, by modifying the differentiation process of airway progenitor cells.

7 ACKNOWLEDGEMENTS

I want to thank Claudia Staab-Weijnitz and Oliver Eickelberg for their outstanding scientific and personal education. I have always been treated with fairness and respect and was supported greatly in times of frustration. My wish to continue scientific training arose from your mentorship in these first steps in academic medicine.

I also want to thank all members of the Eickelberg Lab, Comprehensive Pneumology Center, and Kaminski Lab, specifically Larissa Knüppel, Elisabeth Hennen, Thomas van Pul, Andrea Schamberger, Katharina Heinzelmann, Gerald Burgstaller, Michael Gerckens, Isis Fernandez, Daniela Dietel, Ernestine Lusse, Argyris Tzouvelekis, Guoying Yu, Giuseppe DeIuliis, Koji Sakamoto, and Naftali Kaminski. I further want to thank the team of the CPC research school, Claudia Staab-Weijnitz, Melanie Königshoff, Doreen Franke, Anjte Brand and Hoeke Baarsma, as well as all fellow PhD and medical students, who trained with me. Thank you all for making this research project such a fantastic professional and personal experience.

Lastly, I want to thank my family for your unconditional and loving support throughout my entire life. This work is dedicated to you.

8 APPENDIX

8.1 ABBREVIATIONS

Δ Ct	delta cycle of threshold
∞	infinite
#	number of
°C	degree celsius
αSMA	alpha smooth muscle actin
A	adenosine
acTub	acetylated Tubulin
ALI	air liquid interface
bAct	beta actin
BAL	bronchoalveolar lavage
BCA	bicinchoninic acid
BEBM	basal epithelial cell basal medium
BEGM	basal epithelial cell growth medium
BiP	binding immunoglobulin protein
BIPF	bleomycin-induced pulmonary fibrosis
BrdU	bromdesoxyuridin
BSA	bovine serum albumin
C	cytosine
Cat#	catalogue number
CC10	clara cell 10 kD protein
cDNA	complementary DNA
cm	centimeter
CO_2	carbon dioxide
COL	collagen
CPC	Comprehensive Pneumology Center
CRTAP	cartilage associated protein
CT	computed tomography
ctrl	control
d	day
Da	dalton
DAPI	4',6-Diamidin-2-phenylindol
ddH_2O	double distilled water
DLCO	diffusing capacity of the lung for carbon monoxide
DMEM	Dulbecco's Modified Eagle Medium
DMSO	dimethylsulfoxid

DNA	deoxyribonucleic acid
dNTP	deoxynucleotide triphosphates
DPBS	Dulbecco's Phosphate-Buffered Saline
DTT	dithiothreitol
e.g.	exempli gratia
ECL	enhanced chemoluminescence
ECM	extracellular matrix
EDTA	ethylenediaminetetraacetic acid
ER	endoplasmic reticulum
et al.	et alia
FBS	fetal bovine serum
FFPE	formaline fixed paraffine embedded
FKBP10	FK506-binding protein 10
FVC	forced vital capacity
g	gram
g	gravitational force
G	guanosine
GAPDH	glyceraldehyde phosphate dehydrogenase
h	hour
HBSS	Hanks' balanced salt solution
HBSS	HEPES buffered saline solution
HC	healthy control
HCl	hydrochloric acid
HEPES	2-[4-(2-hydroxyethyl)piperazin-1-yl]ethanesulfonic acid
HER2	human epidermal growth factor receptor 2
HIF-1α	hypoxia-inducible factor 1 alpha
HK2 cells	human kidney 2 cells
HMBS	hydroxymethylbilane synthase
HPRT	hypoxanthine-guanine phosphoribosyltransferase
HRP	horseradish peroxidase
IF	immunofluorescence
IgG	immunoglobulin G
IL-10	interleukin 10
ILD	interstitial lung disease
inh	inhibitor
IPF	idiopathic pulmonary fibrosis
k	kilo
KD	knockdown
Krt14	cytokeratin-14

Krt5	cytokeratin-5
l	liter
LT	lung tissue
LTRC	Lung Tissue Research Consortium
µ	micro
m	milli
M	molar
$MgCl_2$	magnesium chloride
min	minute
miR	micro RNA
mRNA	messenger RNA
Muc5AC	mucin 5AC
Muc5B	mucin 5B
n	nano
N	number of individual experiments
n/s	not specified
NaCl	sodium chloride
NCBI	National Center for Biotechnology Information
NP-40	nonidet P-40
p	pico
p	p-value
P3H1	prolyl-3-hydroxylase 1, LEPRE1
P3H2	prolyl-3-hydroxylase 2, LEPREL1
P4HA1	prolyl-4-hydroxylase α-1
p63	transformation-related protein 63
PAGE	polyacrylamide gel electrophoresis
PBS	phosphate-buffered saline
PCNA	proliferating cell nuclear antigen
PCR	polymerase chain reaction
PDGF-R	platelet-derived growth factor receptor
pen	penicillin
PFA	paraformaldehyde
pHBECs	primary human bronchial epithelial cells
phLF	primary human lung fibroblast
prec	precursor
PVDF	polyvinylidene fluoride
q(RT)-PCR	quantitative (real-time) polymerase chain reaction
RIPA	radioimmunoprecipitation assay buffer
RNA	ribonucleic acid

rpm	revolutions per minute
RT	reverse transcriptase
scrb	scrambled control
SDS	sodium dodecyl sulfate
sec	second
SEM	standard error of the mean
SERCA	sarcoplasmic / endoplasmic reticulum Ca2+ ATPase
siRNA	small interfering RNA
strep	streptomycin
T	thymidine
TBS	tris-buffered saline
TBS-T	tris-buffered saline with tween
TG	thapsigargin
TGFß	transforming growth factor beta
TM	transwell membrane
TM	tunicamycin
Tris	tris(hydroxymethyl)aminomethane
U	unit
U	uracil
UIP	usual interstitial pneumonia
UPR	unfolded protein response
UTR	untranslated region
V	volt
VEGF-R	vascular endothelial growth factor receptor
X	times (multitude of)

8.2 LIST OF FIGURES

FIGURE 1: *IN VITRO* DIFFERENTIATION OF PRIMARY HUMAN BRONCHIAL EPITHELIAL CELLS INTO A MUCOCILIARY EPITHELIUM. 20
FIGURE 2: ANTIBODY AND SILENCER-RNA EVALUATION IN PHLF. 30
FIGURE 3: COLLAGEN HYDROXYLASES IN IPF. 32
FIGURE 4: IF-STAININGS OF IPF AND HC TISSUE. 33
FIGURE 5: IF-STAININGS IN SERIAL CUTS OF IPF AND HC LUNG TISSUE. 34
FIGURE 6: DIFFERENTIATION OF PHEBCS USING THE AIR-LIQUID-INTERFACE MODEL. 35

FIGURE 7: P3H1 PROTEIN DETECTION IN ER-STRESS-CHALLENGED PHBECS. 36
FIGURE 8: P3H1 PROTEIN AND TRANSCRIPT DETECTION IN TGFβ-TREATED PHBECS. 37
FIGURE 9: REGULATION OF P3H1 PROTEIN AND MRNA BY MIR29B INHIBITOR AND PRECURSOR. 39
FIGURE 10: P3H1 AND MIR29B TRANSCRIPT AND COLLAGEN DETECTION IN TGFβ-TREATED PHBECS. 40
FIGURE 11: P3H1 KNOCKDOWN IN DIFFERENTIATING PHBECS. 41
FIGURE 12: P3H1 KNOCKDOWN IN SUBMERGED PHBECS. 42
FIGURE 13: EVALUATION OF P63 IN P3H1-DEPLETED AND TGFβ-TREATED PHBECS. 44
FIGURE 14: PROLIFERATION IN P3H1-DEPLETED PHBECS. 45

8.3 LIST OF TABLES

TABLE 1: LABORATORY EQUIPMENT 9
TABLE 2: SOFTWARE 10
TABLE 3: CHEMICALS AND REAGENTS 10
TABLE 4: KITS 12
TABLE 5: CELLS 12
TABLE 6: MEDIA 13
TABLE 7: CONSUMABLES 13
TABLE 8: MRNA PRIMER 14
TABLE 9: MICRORNA PRIMER 14
TABLE 10: SIRNA TRANSFECTION REAGENTS 15
TABLE 11: MICRORNA TRANSFECTION REAGENTS 15
TABLE 12: PRIMARY ANTIBODIES FOR WESTERN BLOT 15
TABLE 13: SECONDARY ANTIBODIES FOR WESTERN BLOT 16
TABLE 14: PRIMARY ANTIBODIES FOR IF-STAINING OF LUNG TISSUE AND TRANSWELL MEMBRANES 16
TABLE 15: SECONDARY ANTIBODIES FOR IF-STAINING OF LUNGE TISSUE AND TRANSWELL MEMBRANES 16
TABLE 16: BUFFERS AND RECIPES 17
TABLE 17: LIGHT CYCLER PROTOCOL FOR SYBR GREEN BASED QRT-PCR 24
TABLE 18: LIGHT CYCLER PROTOCOL FOR 1-STEP REVERSE TRANSCRIPTION AND QRT-PCR 25
TABLE 19: LIGHT CYCLER PROTOCOL FOR QRT-PCR OF MICRO-RNA SAMPLES 26

8.4 PUBLICATIONS AND PRESENTATIONS

8.4.1 PUBLICATIONS

Karolina Pijadina, Leonhard Binzenhöfer, Juliane Merl-Pham, Trayambak Basak, Andrea Schamberger, Elisabeth Hennen, Natalia Cabeza-Boeddinghaus, Rudolf Hatz, Jürgen Behr, Naftali Kaminski, Stefanie Hauck, Hans Peter Bächinger, Roberto Vanacore, Oliver Eickelberg, Claudia Staab-Weijnitz. **Collagen Prolyl-3-Hydroxylase 1 regulates TGF-beta-induced protein synthesis of type I collagen and fibronectin in bronchial epithelial cells** *(preliminary title)*

-in preparation-

8.4.2 ORAL PRESENTATIONS

December 2015: *P3H1 in idiopathic pulmonary fibrosis*, CPC Research School Symposium, Munich, Germany

March 2016: *P3H1 in idiopathic pulmonary fibrosis*, Kaminski Lab Project Presentation, New Heaven, USA

9 EIDESSTATTLICHE ERKLÄRUNG

Hiermit erkläre ich, Leonhard Binzenhöfer, an Eides statt, dass ich die vorliegende Dissertation mit dem Titel *„Prolyl-3-Hydroxylase 1 in Idiopathic pulmonary fibrosis“* selbstständig angefertigt habe, mich außer der angegebenen keiner weiteren Hilfsmittel bedient und alle Erkenntnisse, die ich aus dem Schrifttum ganz oder annähernd übernommen sind, als solche kenntlich gemacht und nach ihrer Herkunft unter Bezeichnung der Fundstelle einzeln nachgewiesen habe.

Ich erkläre des Weiteren, dass die hier vorliegende Dissertation nicht in gleicher oder in ähnlicher Form bei einer anderen Stelle zur Erlangung eines akademischen Grades eingereicht wurde.

München, den 10.10.2020 Leonhard Binzenhöfer

10 REFERENCES

1. Behr, J. *et al.* S2K-Leitlinie zur Diagnostik und Therapie der idiopathischen Lungenfibrose. *Pneumologie (Stuttgart, Germany)* **67,** 81–111; 10.1055/s-0032-1326009 (2013).

2. Cottin, V. *et al.* Presentation, diagnosis and clinical course of the spectrum of progressive-fibrosing interstitial lung diseases. *European respiratory review : an official journal of the European Respiratory Society* **27**; 10.1183/16000617.0076-2018 (2018).

3. Hutchinson, J., Fogarty, A., Hubbard, R. & McKeever, T. Global incidence and mortality of idiopathic pulmonary fibrosis: a systematic review. *The European respiratory journal* **46,** 795–806; 10.1183/09031936.00185114 (2015).

4. Nalysnyk, L., Cid-Ruzafa, J., Rotella, P. & Esser, D. Incidence and prevalence of idiopathic pulmonary fibrosis: review of the literature. *European respiratory review : an official journal of the European Respiratory Society* **21,** 355–361; 10.1183/09059180.00002512 (2012).

5. Duchemann, B. *et al.* Prevalence and incidence of interstitial lung diseases in a multi-ethnic county of Greater Paris. *The European respiratory journal* **50**; 10.1183/13993003.02419-2016 (2017).

6. Raghu, G. *et al.* Diagnosis of Idiopathic Pulmonary Fibrosis. An Official ATS/ERS/JRS/ALAT Clinical Practice Guideline. *American journal of respiratory and critical care medicine* **198,** e44-e68; 10.1164/rccm.201807-1255ST (2018).

7. Plantier, L. *et al.* Physiology of the lung in idiopathic pulmonary fibrosis. *European respiratory review : an official journal of the European Respiratory Society* **27**; 10.1183/16000617.0062-2017 (2018).

8. Ley, B., Collard, H. R. & King, T. E. Clinical course and prediction of survival in idiopathic pulmonary fibrosis. *American journal of respiratory and critical care medicine* **183,** 431–440; 10.1164/rccm.201006-0894CI (2011).

9. Raghu, G. *et al.* An Official ATS/ERS/JRS/ALAT Clinical Practice Guideline: Treatment of Idiopathic Pulmonary Fibrosis. An Update of the 2011 Clinical Practice Guideline. *American journal of respiratory and critical care medicine* **192,** e3-19; 10.1164/rccm.201506-1063ST (2015).

10. Lancaster, L. *et al.* Safety and survival data in patients with idiopathic pulmonary fibrosis treated with nintedanib: pooled data from six clinical trials. *BMJ open respiratory research* **6,** e000397; 10.1136/bmjresp-2018-000397 (2019).

11. Margaritopoulos, G. A. *et al.* Pirfenidone improves survival in IPF: results from a real-life study. *BMC pulmonary medicine* **18,** 177; 10.1186/s12890-018-0736-z (2018).

12. King, T. E. *et al.* A phase 3 trial of pirfenidone in patients with idiopathic pulmonary fibrosis. *The New England journal of medicine* **370,** 2083–2092; 10.1056/NEJMoa1402582 (2014).

13. Richeldi, L. *et al.* Efficacy and safety of nintedanib in idiopathic pulmonary fibrosis. *The New England journal of medicine* **370,** 2071–2082; 10.1056/NEJMoa1402584 (2014).

14. Conte, E. *et al.* Effect of pirfenidone on proliferation, TGF-β-induced myofibroblast differentiation and fibrogenic activity of primary human lung fibroblasts. *European journal of pharmaceutical sciences : official journal of the European Federation for Pharmaceutical Sciences* **58,** 13–19; 10.1016/j.ejps.2014.02.014 (2014).

15. Knüppel, L. *et al.* A Novel Antifibrotic Mechanism of Nintedanib and Pirfenidone. Inhibition of Collagen Fibril Assembly. *American journal of respiratory cell and molecular biology* **57,** 77–90; 10.1165/rcmb.2016-0217OC (2017).

16. Schaefer, C. J., Ruhrmund, D. W., Pan, L., Seiwert, S. D. & Kossen, K. Antifibrotic activities of pirfenidone in animal models. *European respiratory review : an official journal of the European Respiratory Society* **20,** 85–97; 10.1183/09059180.00001111 (2011).

17. Wollin, L. *et al.* Mode of action of nintedanib in the treatment of idiopathic pulmonary fibrosis. *The European respiratory journal* **45,** 1434–1445; 10.1183/09031936.00174914 (2015).

18. Shoulders, M. D. & Raines, R. T. Collagen structure and stability. *Annual review of biochemistry* **78,** 929–958; 10.1146/annurev.biochem.77.032207.120833 (2009).

19. RICH, A. & CRICK, F. H. The structure of collagen. *Nature* **176,** 915–916; 10.1038/176915a0 (1955).

20. Yamauchi, M. & Sricholpech, M. Lysine post-translational modifications of collagen. *Essays in biochemistry* **52,** 113–133; 10.1042/bse0520113 (2012).

21. Vranka, J. A., Sakai, L. Y. & Bächinger, H. P. Prolyl 3-hydroxylase 1, enzyme characterization and identification of a novel family of enzymes. *The Journal of Biological Chemistry* **279,** 23615–23621; 10.1074/jbc.M312807200 (2004).

22. Knudsen, L. & Ochs, M. The micromechanics of lung alveoli: structure and function of surfactant and tissue components. *Histochemistry and cell biology* **150,** 661–676; 10.1007/s00418-018-1747-9 (2018).

23. Snijder, J., Peraza, J., Padilla, M., Capaccione, K. & Salvatore, M. M. Pulmonary fibrosis: a disease of alveolar collapse and collagen deposition. *Expert review of respiratory medicine* **13,** 615–619; 10.1080/17476348.2019.1623028 (2019).

24. Fernandez, I. E. & Eickelberg, O. The impact of TGF-β on lung fibrosis: from targeting to biomarkers. *Proceedings of the American Thoracic Society* **9,** 111–116; 10.1513/pats.201203-023AW (2012).

25. Walton, K. L., Johnson, K. E. & Harrison, C. A. Targeting TGF-β Mediated SMAD Signaling for the Prevention of Fibrosis. *Frontiers in pharmacology* **8,** 461; 10.3389/fphar.2017.00461 (2017).

26. Chaudhary, N. I. *et al.* Inhibition of PDGF, VEGF and FGF signalling attenuates fibrosis. *The European respiratory journal* **29,** 976–985; 10.1183/09031936.00152106 (2007).

27. Barratt, S. L., Flower, V. A., Pauling, J. D. & Millar, A. B. VEGF (Vascular Endothelial Growth Factor) and Fibrotic Lung Disease. *International Journal of Molecular Sciences* **19**; 10.3390/ijms19051269 (2018).

28. Murray, L. A. *et al.* Antifibrotic role of vascular endothelial growth factor in pulmonary fibrosis. *JCI insight* **2**; 10.1172/jci.insight.92192 (2017).

29. MacKenzie, B. *et al.* Increased FGF1-FGFRc expression in idiopathic pulmonary fibrosis. *Respiratory research* **16,** 83; 10.1186/s12931-015-0242-2 (2015).

30. Aono, Y. *et al.* Role of platelet-derived growth factor/platelet-derived growth factor receptor axis in the trafficking of circulating fibrocytes in pulmonary fibrosis. *American journal of respiratory cell and molecular biology* **51,** 793–801; 10.1165/rcmb.2013-0455OC (2014).

31. Noskovičová, N., Petřek, M., Eickelberg, O. & Heinzelmann, K. Platelet-derived growth factor signaling in the lung. From lung development and disease to clinical studies. *American journal of respiratory cell and molecular biology* **52,** 263–284; 10.1165/rcmb.2014-0294TR (2015).

32. Burgstaller, G. *et al.* The instructive extracellular matrix of the lung: basic composition and alterations in chronic lung disease. *The European respiratory journal* **50**; 10.1183/13993003.01805-2016 (2017).

33. UniProt. UniProtKB - Q32P28 (P3H1_HUMAN). Available at https://www.uniprot.org/uniprot/Q32P28 (2019).

34. UniProt. UniProtKB - O75718 (CRTAP_HUMAN). Available at https://www.uniprot.org/uniprot/O75718 (2019).

35. UniProt. UniProtKB - Q8IVL5 (P3H2_HUMAN). Available at https://www.uniprot.org/uniprot/Q8IVL5 (2019).

36. Hudson, D. M. & Eyre, D. R. Collagen prolyl 3-hydroxylation: a major role for a minor post-translational modification? *Connective tissue research* **54,** 245–251; 10.3109/03008207.2013.800867 (2013).

37. Cabral, W. A. *et al.* Prolyl 3-hydroxylase 1 deficiency causes a recessive metabolic bone disorder resembling lethal/severe osteogenesis imperfecta. *Nature genetics* **39,** 359–365; 10.1038/ng1968 (2007).

38. Morello, R. *et al.* CRTAP is required for prolyl 3- hydroxylation and mutations cause recessive osteogenesis imperfecta. *Cell* **127,** 291–304; 10.1016/j.cell.2006.08.039 (2006).

39. Vranka, J. A. *et al.* Prolyl 3-hydroxylase 1 null mice display abnormalities in fibrillar collagen-rich tissues such as tendons, skin, and bones. *The Journal of Biological Chemistry* **285,** 17253–17262; 10.1074/jbc.M110.102228 (2010).

40. Willaert, A. *et al.* Recessive osteogenesis imperfecta caused by LEPRE1 mutations: clinical documentation and identification of the splice form responsible for prolyl 3-hydroxylation. *Journal of medical genetics* **46,** 233–241; 10.1136/jmg.2008.062729 (2009).

41. Jones, M. G. *et al.* Nanoscale dysregulation of collagen structure-function disrupts mechano-homeostasis and mediates pulmonary fibrosis. *eLife* **7**; 10.7554/eLife.36354 (2018).

42. Giménez, A. *et al.* Dysregulated Collagen Homeostasis by Matrix Stiffening and TGF-β1 in Fibroblasts from Idiopathic Pulmonary Fibrosis Patients: Role of FAK/Akt. *International Journal of Molecular Sciences* **18**; 10.3390/ijms18112431 (2017).

43. Schiller, H. B. *et al.* Time- and compartment-resolved proteome profiling of the extracellular niche in lung injury and repair. *Molecular systems biology* **11,** 819; 10.15252/msb.20156123 (2015).

44. Staab-Weijnitz, C. A. *et al.* FK506-Binding Protein 10, a Potential Novel Drug Target for Idiopathic Pulmonary Fibrosis. *American journal of respiratory and critical care medicine* **192,** 455–467; 10.1164/rccm.201412-2233OC (2015).

45. Schamberger, A. C., Staab-Weijnitz, C. A., Mise-Racek, N. & Eickelberg, O. Cigarette smoke alters primary human bronchial epithelial cell differentiation at the air-liquid interface. *Scientific reports* **5,** 8163; 10.1038/srep08163 (2015).

46. Montgomery, R. L. *et al.* MicroRNA mimicry blocks pulmonary fibrosis. *EMBO molecular medicine* **6,** 1347–1356; 10.15252/emmm.201303604 (2014).

47. Liu, T., Los Santos, F. G. de & Phan, S. H. The Bleomycin Model of Pulmonary Fibrosis. *Methods in molecular biology (Clifton, N.J.)* **1627,** 27–42; 10.1007/978-1-4939-7113-8_2 (2017).

48. Tashiro, J. *et al.* Exploring Animal Models That Resemble Idiopathic Pulmonary Fibrosis. *Frontiers in medicine* **4,** 118; 10.3389/fmed.2017.00118 (2017).

49. Schwartz, D. A. IDIOPATHIC PULMONARY FIBROSIS IS A COMPLEX GENETIC DISORDER. *Transactions of the American Clinical and Climatological Association* **127,** 34–45 (2016).

50. Clarke, D. L., Murray, L. A., Crestani, B. & Sleeman, M. A. Is personalised medicine the key to heterogeneity in idiopathic pulmonary fibrosis? *Pharmacology & therapeutics* **169,** 35–46; 10.1016/j.pharmthera.2016.09.010 (2017).

51. Kreuter, M. & Maher, T. Gazing into the crystal ball: can treatment response be predicted in IPF? *The Lancet Respiratory Medicine* **6,** 570–572; 10.1016/S2213-2600(18)30234-0 (2018).

52. Kaminiski N. Idiopathic pulmonary fibrosis. GDS1252 / 98,26 P3H1. Available at https://www.ncbi.nlm.nih.gov/geo/tools/profileGraph.cgi?ID=GDS1252:98%2C26 (2005).

53. Kaminiski N. Idiopathic pulmonary fibrosis. GDS1252 / 52,38 P3H2. Available at https://www.ncbi.nlm.nih.gov/geo/tools/profileGraph.cgi?ID=GDS1252:52%2C38 (2005).

54. Kaminiski N. Idiopathic pulmonary fibrosis. GDS1252 / 34,20 CRTAP. Available at https://www.ncbi.nlm.nih.gov/geo/tools/profileGraph.cgi?ID=GDS1252:34%2C20 (2005).

55. Guo, Y. *et al.* How is mRNA expression predictive for protein expression? A correlation study on human circulating monocytes. *Acta biochimica et biophysica Sinica* **40,** 426–436; 10.1111/j.1745-7270.2008.00418.x (2008).

56. Parker, M. W. *et al.* Fibrotic extracellular matrix activates a profibrotic positive feedback loop. *The Journal of clinical investigation* **124,** 1622–1635; 10.1172/JCI71386 (2014).

57. Li, Y. *et al.* Severe lung fibrosis requires an invasive fibroblast phenotype regulated by hyaluronan and CD44. *The Journal of experimental medicine* **208,** 1459–1471; 10.1084/jem.20102510 (2011).

58. Hackett, N. R. *et al.* The human airway epithelial basal cell transcriptome. *PloS one* **6,** e18378; 10.1371/journal.pone.0018378 (2011).

59. van der Flier, A. & Sonnenberg, A. Function and interactions of integrins. *Cell and tissue research* **305,** 285–298; 10.1007/s004410100417 (2001).

60. Prasse, A. *et al.* BAL Cell Gene Expression Is Indicative of Outcome and Airway Basal Cell Involvement in Idiopathic Pulmonary Fibrosis. *American journal of respiratory and critical care medicine* **199,** 622–630; 10.1164/rccm.201712-2551OC (2019).

61. Wolters, P. J. *et al.* Time for a change: is idiopathic pulmonary fibrosis still idiopathic and only fibrotic? *The Lancet. Respiratory medicine* **6,** 154–160; 10.1016/S2213-2600(18)30007-9 (2018).

62. Tsuji, T., Aoshiba, K. & Nagai, A. Cigarette smoke induces senescence in alveolar epithelial cells. *American journal of respiratory cell and molecular biology* **31,** 643–649; 10.1165/rcmb.2003-0290OC (2004).

63. Seibold, M. A. *et al.* A common MUC5B promoter polymorphism and pulmonary fibrosis. *The New England journal of medicine* **364,** 1503–1512; 10.1056/NEJMoa1013660 (2011).

64. Camelo, A., Dunmore, R., Sleeman, M. A. & Clarke, D. L. The epithelium in idiopathic pulmonary fibrosis: breaking the barrier. *Frontiers in pharmacology* **4,** 173; 10.3389/fphar.2013.00173 (2014).

65. Clarke, D. L., Carruthers, A. M., Mustelin, T. & Murray, L. A. Matrix regulation of idiopathic pulmonary fibrosis: the role of enzymes. *Fibrogenesis & tissue repair* **6,** 20; 10.1186/1755-1536-6-20 (2013).

66. Jonsdottir, H. R. *et al.* Basal cells of the human airways acquire mesenchymal traits in idiopathic pulmonary fibrosis and in culture. *Laboratory investigation; a journal of technical methods and pathology* **95,** 1418–1428; 10.1038/labinvest.2015.114 (2015).

67. Kim, K. K. *et al.* Alveolar epithelial cell mesenchymal transition develops in vivo during pulmonary fibrosis and is regulated by the extracellular matrix. *Proceedings of the National Academy of Sciences of the United States of America* **103,** 13180–13185; 10.1073/pnas.0605669103 (2006).

68. J.E. McDonough, S.E. Verleden, J. Verschakelen, W. Wuyts, B.M. Vanaudenaerde. The Structural Origin of Honeycomb Cysts in IPF. Available at https://www.atsjournals.org/doi/abs/10.1164/ajrccm-conference.2018.197.1_MeetingAbstracts.A6388https://www.atsjournals.org/doi/abs/10.1164/ajrccm-conference.2018.197.1_MeetingAbstracts.A6388 (2018).

69. Chilosi, M. *et al.* Abnormal re-epithelialization and lung remodeling in idiopathic pulmonary fibrosis: the role of deltaN-p63. *Laboratory investigation; a journal of technical methods and pathology* **82,** 1335–1345; 10.1097/01.lab.0000032380.82232.67 (2002).

70. Hwang, J. & Qi, L. Quality Control in the Endoplasmic Reticulum: Crosstalk between ERAD and UPR pathways. *Trends in biochemical sciences* **43,** 593–605; 10.1016/j.tibs.2018.06.005 (2018).

71. Chami, M. *et al.* SERCA1 truncated proteins unable to pump calcium reduce the endoplasmic reticulum calcium concentration and induce apoptosis. *The Journal of cell biology* **153,** 1301–1314; 10.1083/jcb.153.6.1301 (2001).

72. Tzouvelekis, A. *et al.* Comparative expression profiling in pulmonary fibrosis suggests a role of hypoxia-inducible factor-1alpha in disease pathogenesis. *American journal of respiratory and critical care medicine* **176,** 1108–1119; 10.1164/rccm.200705-683OC (2007).

73. Maitra, M., Wang, Y., Gerard, R. D., Mendelson, C. R. & Garcia, C. K. Surfactant Protein A2 Mutations Associated with Pulmonary Fibrosis Lead to Protein Instability and Endoplasmic Reticulum Stress*. *The Journal of Biological Chemistry* **285,** 22103–22113; 10.1074/jbc.M110.121467 (2010).

74. Bueno, M. *et al.* PINK1 deficiency impairs mitochondrial homeostasis and promotes lung fibrosis. *The Journal of clinical investigation* **125,** 521–538; 10.1172/JCI74942 (2014).

75. Burman, A., Tanjore, H. & Blackwell, T. S. Endoplasmic reticulum stress in pulmonary fibrosis. *Matrix biology : journal of the International Society for Matrix Biology* **68-69,** 355–365; 10.1016/j.matbio.2018.03.015 (2018).

76. Wolters, P. J., Collard, H. R. & Jones, K. D. Pathogenesis of Idiopathic Pulmonary Fibrosis. *Annual review of pathology* **9,** 157–179; 10.1146/annurev-pathol-012513-104706 (2013).

77. Kropski, J. A. & Blackwell, T. S. Endoplasmic reticulum stress in the pathogenesis of fibrotic disease. *The Journal of clinical investigation* **128,** 64–73; 10.1172/JCI93560.

78. Tanjore, H. *et al.* Alveolar epithelial cells undergo epithelial-to-mesenchymal transition in response to endoplasmic reticulum stress. *The Journal of Biological Chemistry* **286,** 30972–30980; 10.1074/jbc.M110.181164 (2011).

79. Tanjore, H., Blackwell, T. S. & Lawson, W. E. Emerging evidence for endoplasmic reticulum stress in the pathogenesis of idiopathic pulmonary fibrosis. *American Journal of Physiology - Lung Cellular and Molecular Physiology* **302,** L721-9; 10.1152/ajplung.00410.2011 (2012).

80. Schröder, M. & Kaufman, R. J. The mammalian unfolded protein response. *Annual review of biochemistry* **74,** 739–789; 10.1146/annurev.biochem.73.011303.074134 (2005).

81. Baarsma, H. A. & Königshoff, M. 'WNT-er is coming': WNT signalling in chronic lung diseases. *Thorax* **72,** 746–759; 10.1136/thoraxjnl-2016-209753 (2017).

82. Saito, A., Horie, M. & Nagase, T. TGF-β Signaling in Lung Health and Disease. *International Journal of Molecular Sciences* **19**; 10.3390/ijms19082460 (2018).

83. Drakopanagiotakis, F., Xifteri, A., Polychronopoulos, V. & Bouros, D. Apoptosis in lung injury and fibrosis. *The European respiratory journal* **32,** 1631–1638; 10.1183/09031936.00176807 (2008).

84. Hagimoto, N. *et al.* TGF-beta 1 as an enhancer of Fas-mediated apoptosis of lung epithelial cells. *Journal of immunology (Baltimore, Md. : 1950)* **168,** 6470–6478; 10.4049/jimmunol.168.12.6470 (2002).

85. Bergeron, A. *et al.* Cytokine profiles in idiopathic pulmonary fibrosis suggest an important role for TGF-beta and IL-10. *The European respiratory journal* **22,** 69–76; 10.1183/09031936.03.00014703 (2003).

86. Biocolor life science assays. Sircol Soluble COLLAGEN Assay Manual. Available at https://www.biocolor.co.uk/site/wp-content/uploads/2016/04/sircol-soluble-assay.pdf (2015).

87. Cushing, L., Kuang, P. & Lü, J. The role of miR-29 in pulmonary fibrosis. *Biochemistry and cell biology = Biochimie et biologie cellulaire* **93,** 109–118; 10.1139/bcb-2014-0095 (2015).

88. Pandit, K. V., Milosevic, J. & Kaminski, N. MicroRNAs in idiopathic pulmonary fibrosis. *Translational research : the journal of laboratory and clinical medicine* **157,** 191–199; 10.1016/j.trsl.2011.01.012 (2011).

89. Du, B. *et al.* High glucose down-regulates miR-29a to increase collagen IV production in HK-2 cells. *FEBS letters* **584,** 811–816; 10.1016/j.febslet.2009.12.053 (2010).

90. Cushing, L. *et al.* miR-29 Is a Major Regulator of Genes Associated with Pulmonary Fibrosis. *American journal of respiratory cell and molecular biology* **45,** 287–294; 10.1165/rcmb.2010-0323OC (2010).

91. Roderburg, C. *et al.* Micro-RNA profiling reveals a role for miR-29 in human and murine liver fibrosis. *Hepatology (Baltimore, Md.)* **53,** 209–218; 10.1002/hep.23922 (2011).

92. Qin, W. *et al.* TGF-β/Smad3 Signaling Promotes Renal Fibrosis by Inhibiting miR-29. *Journal of the American Society of Nephrology : JASN* **22,** 1462–1474; 10.1681/ASN.2010121308 (2011).

93. DIANA TOOLS MicroRNA target prediction. ENSG00000117385. Available at http://diana.imis.athena-innovation.gr/DianaTools/index.php?r=microT_CDS/results&keywords=ENSG00000117385&genes=ENSG00000117385%20&mirnas=&descr=&threshold=0.7&page=2 (2018).

94. Target Scan Human. Human LEPRE1 ENST00000236040.4 3' UTR length: 835. Available at http://www.targetscan.org/cgi-bin/targetscan/vert_72/view_gene.cgi?rs=ENST00000236040.4&taxid=9606&members=miR-29-3p&showcnc=0&shownc=0&showncf1=&showncf2=&subset=1 (2018).

95. Leoni, G. *et al.* Ex Vivo and In Vivo Lentivirus-Mediated Transduction of Airway Epithelial Progenitor Cells. *Current gene therapy* **15,** 581–590; 10.2174/1566523215666151016123625 (2015).

96. Yang, A. *et al.* p63, a p53 homolog at 3q27-29, encodes multiple products with transactivating, death-inducing, and dominant-negative activities. *Molecular cell* **2,** 305–316; 10.1016/s1097-2765(00)80275-0 (1998).

97. Yang, A. & McKeon, F. P63 and P73: P53 mimics, menaces and more. *Nature reviews. Molecular cell biology* **1,** 199–207; 10.1038/35043127 (2000).

98. Crum, C. P. & McKeon, F. D. p63 in epithelial survival, germ cell surveillance, and neoplasia. *Annual review of pathology* **5,** 349–371; 10.1146/annurev-pathol-121808-102117 (2010).

99. Arason, A. J. *et al.* deltaNp63 has a role in maintaining epithelial integrity in airway epithelium. *PloS one* **9,** e88683; 10.1371/journal.pone.0088683 (2014).

100. Yoh, K. & Prywes, R. Pathway Regulation of p63, a Director of Epithelial Cell Fate. *Frontiers in endocrinology* **6,** 51; 10.3389/fendo.2015.00051 (2015).

101. Yang, A. *et al.* p63 is essential for regenerative proliferation in limb, craniofacial and epithelial development. *Nature* **398,** 714–718; 10.1038/19539 (1999).

102. Mills, A. A. *et al.* p63 is a p53 homologue required for limb and epidermal morphogenesis. *Nature* **398,** 708–713; 10.1038/19531 (1999).

103. Romano, R.-A. *et al.* ΔNp63 knockout mice reveal its indispensable role as a master regulator of epithelial development and differentiation. *Development (Cambridge, England)* **139,** 772–782; 10.1242/dev.071191 (2012).

104. Warner, S. M. B. *et al.* Transcription factor p63 regulates key genes and wound repair in human airway epithelial basal cells. *American journal of respiratory cell and molecular biology* **49,** 978–988; 10.1165/rcmb.2012-0447OC (2013).

105. Xiong, G. *et al.* Collagen prolyl 4-hydroxylase 1 is essential for HIF-1α stabilization and TNBC chemoresistance. *Nature communications* **9,** 4456; 10.1038/s41467-018-06893-9 (2018).

106. Hubbi, M. E. & Semenza, G. L. Regulation of cell proliferation by hypoxia-inducible factors. *American journal of physiology. Cell physiology* **309,** C775-82; 10.1152/ajpcell.00279.2015 (2015).

107. Shah, R. *et al.* The prolyl 3-hydroxylases P3H2 and P3H3 are novel targets for epigenetic silencing in breast cancer. *British journal of cancer* **100,** 1687–1696; 10.1038/sj.bjc.6605042 (2009).

108. Wang, J. *et al.* LEPREL1 Expression in Human Hepatocellular Carcinoma and Its Suppressor Role on Cell Proliferation. *Gastroenterology research and practice* **2013,** 109759; 10.1155/2013/109759 (2013).

109. Kaul, S. C., Sugihara, T., Yoshida, A., Nomura, H. & Wadhwa, R. Gros1, a potential growth suppressor on chromosome 1: its identity to basement membrane-associated proteoglycan, leprecan. *Oncogene* **19,** 3576–3583; 10.1038/sj.onc.1203696 (2000).

110. Smirnova, N. F. *et al.* Detection and quantification of epithelial progenitor cell populations in human healthy and IPF lungs. *Respiratory research* **17,** 83; 10.1186/s12931-016-0404-x (2016).

111. Ryan, R. M., Mineo-Kuhn, M. M., Kramer, C. M. & Finkelstein, J. N. Growth factors alter neonatal type II alveolar epithelial cell proliferation. *The American journal of physiology* **266,** L17-22; 10.1152/ajplung.1994.266.1.L17 (1994).